bioRxiv preprint doi: https://doi.org/10.1101/253096; this version posted January 24, 2018. The copyright holder for this preprint (which was not certified by peer review) is the author/funder, who has granted bioRxiv a license to display the preprint in perpetuity. It is made available under aCC-BY-NC-ND 4.0 International license.

Structure-guided design of a cell penetrating peptide preventing cAMP modulation of HCN channels

Andrea Saponaro[1], Francesca Cantini[2], Alessandro Porro[1], Annalisa Bucchi[1], Dario Di Francesco[1], Vincenzo Maione[2], Chiara Donadoni[1], Bianca Introini[1], Pietro Mesirca[3], Matteo E. Mangoni[3], Gerhard Thiel[4], Lucia Banci[2,5], Bina Santoro[6], Anna Moroni[1,7]

[1]Department of Biosciences University of Milan, Italy;

[2]Centro Risonanze Magnetiche (CERM) and Department of Chemistry, University of Florence, Italy;

[3]Département de Physiologie, Institut de Genomique Fonctionnelle, LabEx ICST, UMR-5203, Centre national de la recherche scientifique, F-34094, Montpellier, France.

[4]Department of Biology, TU-Darmstadt, Darmstadt, Germany;

[5]Institute of Neurosciences, Consiglio Nazionale delle Ricerche, Florence, Italy

[6]Department of Neuroscience, Columbia University, New York, USA;

[7]Institute of Biophysics, Consiglio Nazionale delle Ricerche, Milan, Italy.

* Corresponding author: Anna Moroni, Department of Biosciences, Via Celoria 26, 20133 Milano, Italy, tel. + 39 12 50314826, email: anna.moroni@unimi.it

Running title: **A synthetic regulator of HCN channels**

bioRxiv preprint doi: https://doi.org/10.1101/253096; this version posted January 24, 2018. The copyright holder for this preprint (which was not certified by peer review) is the author/funder, who has granted bioRxiv a license to display the preprint in perpetuity. It is made available under aCC-BY-NC-ND 4.0 International license.

Abstract

The auxiliary subunit TRIP8b prevents cAMP activation of HCN channels by antagonizing its binding to their cyclic-nucleotide binding domain (CNBD). By determining an NMR-derived structure of the complex formed by the HCN2 channel CNBD and a minimal TRIP8b fragment, $TRIP_{nano}$, we show here a bipartite interaction between the peptide and CNBD which prevents cAMP binding in two ways: through direct competition for binding at the distal C-helix of the CNBD; and through an allosteric reduction in cAMP affinity induced by TRIP8b binding to the CNBD N-bundle loop. $TRIP_{nano}$ abolishes cAMP binding in all three isoforms, HCN1, HCN2 and HCN4 and can be used to prevent cAMP stimulation in native f-channels. Application of $TRIP8b_{nano}$, or its delivery via a cell-penetrating sequence, in sinoatrial node myocytes, selectively inhibits beta-adrenergic stimulation of the native I_f current and mimics the physiological concentrations of acetylcholine leading to a 30% reduction in the spontaneus rate of action potential firing.

Keywords: HCN channels/TRIP8b/cAMP/allosteric inhibition/direct competition

bioRxiv preprint doi: https://doi.org/10.1101/253096; this version posted January 24, 2018. The copyright holder for this preprint (which was not certified by peer review) is the author/funder, who has granted bioRxiv a license to display the preprint in perpetuity. It is made available under aCC-BY-NC-ND 4.0 International license.

Introduction

Hyperpolarization-activated cyclic nucleotide-regulated (HCN1-4) channels are the molecular correlate of the I_f/I_h current, which plays a key role in controlling several higher order electrophysiological functions, including dendritic integration and intrinsic rhythmicity both in cardiac and neuronal cells (Robinson & Siegelbaum, 2003). Unique among the voltage-gated ion channel superfamily, HCN channels are modulated by the direct binding of cAMP to their C-terminal CNBD. cAMP binding enhances channel opening upon hyperpolarization via conformational changes in the CNBD that are propagated, through the C-linker domain, to the pore (Wainger *et al*, 2001; Zagotta *et al*, 2003).

In addition to cAMP, HCN channels are regulated by TRIP8b, their brain-specific auxiliary (β) subunit, which modulates channel trafficking and gating (Santoro *et al*, 2009; Zolles *et al*, 2009). TRIP8b binds HCN channels in two distinct sites: the tetratricopeptide repeat (TPR) domain, which binds the last three amino acids (SNL) of HCN channels; and the $TRIP8b_{core}$ domain, which interacts with the HCN channel CNBD domain (Santoro *et al*, 2011). Although TRIP8b is subject to alternative splicing giving rise to nine isoforms with different effects on HCN trafficking (Santoro *et al*, 2009; Piskorowski *et al*, 2011; Lewis *et al*, 2009), all isoforms act in the same way on the electrical activity of HCN channels: they bind to the cAMP-free state of the CNBD and thus antagonize the effect of the ligand on the voltage dependency of the channel (Hu *et al*, 2013).

In previous work, we contributed to elucidating the dual mechanism of action of cAMP and TRIP8b on HCN channels by using a simplified system that included the HCN2 CNBD and the $TRIP8b_{core}$ protein fragments (Saponaro *et al*, 2014). By means of solution NMR spectroscopy we described in atomic detail the cAMP-induced conformational changes occurring in the HCN channel CNBD. These include a major rearrangement of the C-terminal helix of the CNBD (C-helix), which undergoes lateral translation and folding upon

bioRxiv preprint doi: https://doi.org/10.1101/253096; this version posted January 24, 2018. The copyright holder for this preprint (which was not certified by peer review) is the author/funder, who has granted bioRxiv a license to display the preprint in perpetuity. It is made available under aCC-BY-NC-ND 4.0 International license.

cAMP binding; and an upward movement of the N-terminal helical bundle, a helix-turn-helix motif immediately upstream of the CNBD β-roll, which presumably initiates the cAMP-induced facilitation of pore opening. These movements are ostensibly inhibited by TRIP8b binding to both the C-helix and N-terminal helical bundle, thus explaining the allosteric inhibition exerted by TRIP8b on the HCN channel response to cAMP (Hu *et al*, 2013). The above TRIP8b interaction sites were validated by deletion analysis, confirming that both the N-terminal helical bundle and the C-helix are necessary but not sufficient for $TRIP8b_{core}$ binding to the CNBD (Saponaro *et al*, 2014). Despite these findings, several reports have suggested a direct competition mechanism between the two ligands for a common binding region that comprises the C-helix and the phosphate binding cassette, PBC, in the HCN channel CNBD (Han *et al*, 2011; Deberg *et al*, 2015; Bankston *et al*, 2017).

A comprehensive structural model of the complex between TRIP8b and the HCN channel CNBD, which may explain the interaction in atomic detail, is therefore crucial for solving the apparent discrepancies between the two proposed models.

We present here a NMR-based 3D model structure of the complex formed by a minimal TRIP8b fragment and the CNBD of the human HCN2 channel isoform, which provides molecular support for both direct and indirect (allosteric) competition modes exerted by TRIP8b on cAMP binding. $TRIP8b_{nano}$ prevented cAMP stimulation in all HCN isoform tested (HCN1, 2 and 4) and was further employed to manipulate the native I_f current in cardiac pacemaker cells. This result opens the possibility of controlling *in vivo* the cAMP-dependent facilitation of HCN channel opening, which represents the basis for the autonomic regulation of cardiac activity and spontaneous neuronal firing (Robinson & Siegelbaum, 2003).

bioRxiv preprint doi: https://doi.org/10.1101/253096; this version posted January 24, 2018. The copyright holder for this preprint (which was not certified by peer review) is the author/funder, who has granted bioRxiv a license to display the preprint in perpetuity. It is made available under aCC-BY-NC-ND 4.0 International license.

Results

We have previously shown that TRIP8b$_{core}$ (residues 223 - 303 of mouse TRIP8b splice variant 1a4, hereafter TRIP8b) interacts with two elements of the isolated CNBD protein fragment from HCN channels (residues 521 - 672 of human HCN2, hereafter CNBD): the C-helix and the N-bundle loop, a sequence connecting helix E' of the C-linker with helix A of the CNBD (Saponaro *et al*, 2014). Biochemical assays confirmed that each of these two elements i.e. the N-bundle loop and C-helix is necessary but not sufficient for binding (Saponaro *et al*, 2014).

To understand the interaction in atomic detail, we used solution NMR spectroscopy to characterize the structural properties of the CNBD-TRIP8b$_{core}$ complex. However, the NMR spectra of TRIP8b$_{core}$ showed very few signals. In order to improve the quality of the NMR spectra, we reduced the length of the TRIP8b fragment by progressively removing residues at the N- and C-termini with no predicted secondary structure. The truncated peptides were then tested for CNBD binding activity by isothermal titration calorimetry (ITC). We thus identified a 40 amino acid peptide (TRIP8b$_{nano}$, comprising residues 235 – 275 of TRIP8b, Fig 1A) with a binding K_D of 1.5 ± 0.1 µM, a value very similar to the K_D of 1.2 ± 0.1 µM obtained with TRIP8b$_{core}$ (Fig 1B). TRIP8b$_{nano}$ was therefore employed for all subsequent NMR experiments, resulting in a remarkable improvement in the spectral quality and sample stability.

Structural characterization of TRIP8b$_{nano}$ bound to CNBD

The comparison of the ^{1}H-^{15}N HSQC spectra of TRIP8b$_{nano}$ with and without CNBD bound shows that the peptide folds upon interaction with the CNBD. Thus, ^{1}H-^{15}N HSQC spectrum of TRIP8b$_{nano}$ without CNBD shows a limited ^{1}H resonance dispersion characteristic of unstructured proteins (Dyson & Wright, 2004), while a larger number of well-dispersed amide signals appear in the spectrum of the CNBD-bound form (Fig 1C). Importantly, we

bioRxiv preprint doi: https://doi.org/10.1101/253096; this version posted January 24, 2018. The copyright holder for this preprint (which was not certified by peer review) is the author/funder, who has granted bioRxiv a license to display the preprint in perpetuity. It is made available under aCC-BY-NC-ND 4.0 International license.

were now able to assign the backbone chemical shift resonances of TRIP8b$_{nano}$ bound to the CNBD. The φ and ψ dihedral angles obtained from the NMR assignment indicate that the peptide displays two α-helices (stretch L_{238}-E_{250} named helix N and stretch T_{253}-R_{269} named helix C) when bound to CNBD. The helices are separated by two amino acids; three and six residues at the N- and C- termini, respectively, are unstructured (Fig 1D).

Structural characterization of CNBD bound to TRIP8b$_{nano}$

NMR-analysis of the CNBD fragment bound to TRIP8b$_{nano}$ revealed that the interaction with the peptide does not affect the overall fold of the protein. Thus, the CNBD adopts the typical fold of the cAMP-free state, in line with previous evidence that this is the form bound by TRIP8b (Deberg *et al*, 2015; Saponaro *et al*, 2014). More specifically, the secondary structure elements of the cAMP-free CNBD are all conserved in the TRIP8b$_{nano}$–bound CNBD (Fig 2). This finding generally agrees with a recent double electron-electron resonance (DEER) analysis of the CNBD-TRIP8b interaction, which showed that TRIP8b binds to a conformation largely similar to the cAMP-free state (Deberg *et al*, 2015). Despite the overall agreement with the DEER study, the NMR data also reveal a new and unexpected feature of TRIP8b binding to the CNBD. Our results surprisingly show that TRIP8b$_{nano}$ induces, upon binding to the CNBD, a well-defined secondary structure of the distal region of the C-helix (Fig 2). This means that the distal region of the C-helix (residues 657-662), which is unstructured in the free form of the CNBD (Saponaro *et al*, 2014; Lee & MacKinnon, 2017), extends into a helical structure upon ligand binding irrespectively of whether the ligand is cAMP (Saponaro *et al*, 2014; Puljung & Zagotta, 2013; Lee & MacKinnon, 2017) or TRIP8b (Fig 2). In contrast, and very differently from cAMP, which directly contacts the P-helix in the Phosphate Binding cassette (PBC) and causes its folding (Saponaro *et al*, 2014; Lee & MacKinnon, 2017), the NMR data show that TRIP8b$_{nano}$ binding to the CNBD does not induce P-helix formation (Fig 2).

bioRxiv preprint doi: https://doi.org/10.1101/253096; this version posted January 24, 2018. The copyright holder for this preprint (which was not certified by peer review) is the author/funder, who has granted bioRxiv a license to display the preprint in perpetuity. It is made available under aCC-BY-NC-ND 4.0 International license.

Modelling the CNBD-TRIP8b$_{nano}$ complex

Despite the significant improvement in sample stability and NMR spectra quality achieved upon TRIP8b$_{nano}$ binding, we were still unable to assign the side chains of both proteins in the complex and thus could not solve the solution structure of the complex by the canonical NMR procedure. We therefore built a model of the CNBD-TRIP8b$_{nano}$ complex by docking the two NMR-derived structures using the Haddock program (a detailed description of how the respective structures were generated is provided in Materials and Methods and Appendix Table S1).

In order to define the active residues (ambiguous interaction restraints) on the CNBD we used the chemical shift perturbation values as described in Appendix Fig S1. For TRIP8b$_{nano}$, we defined as active a stretch of residues, E_{239}-E_{243}, previously identified as critical for the interaction (Santoro *et al*, 2009, 2011). Output clusters of this first molecular docking calculation (settings can be found in Material and Methods) were further screened for TRIP8b$_{nano}$ orientations in agreement with a previous DEER analysis, which placed TRIP8b residue A_{248} closer to the proximal portion and TRIP8b residue A_{261} closer to the distal portion of the CNBD C-helix (Deberg *et al*, 2015). Remarkably, in all clusters thus selected, residues E_{264} or E_{265} in TRIP8b were found to interact with residues K_{665} or K_{666} of the CNBD (Appendix Fig S2). This finding was notable, because we previously identified K_{665}/K_{666} as being critical for TRIP8b interaction in a biochemical binding assay (Saponaro *et al*, 2014). We thus proceeded to individually mutate each of these four positions, and test their effect on binding affinity through ITC. As expected, reverse charge mutations K_{665}E or K_{666}E (CNBD) as well as E_{264}K or E_{265}K (TRIP8b$_{nano}$) each strongly reduced the CNBD/TRIP8b$_{nano}$ binding affinity (Appendix Fig S3).

Based on these observations, we performed a second molecular docking calculation, including E_{264} and E_{265} as additional active residues for TRIP8b$_{nano}$. This procedure resulted

bioRxiv preprint doi: https://doi.org/10.1101/253096; this version posted January 24, 2018. The copyright holder for this preprint (which was not certified by peer review) is the author/funder, who has granted bioRxiv a license to display the preprint in perpetuity. It is made available under aCC-BY-NC-ND 4.0 International license.

in the model shown in Fig 3, which represents the top-ranking cluster for energetic and scoring function (Appendix Table S2) and was fully validated by mutagenesis analysis as described below. Scrutiny of the model shows that TRIP8b$_{nano}$ binds to both the C-helix and the N-bundle loop (Fig 3A). Binding to the C-helix is mainly guided by electrostatic interactions between the negative charges on TRIP8b$_{nano}$, and the positive charges on the CNBD (Fig 3A). As shown in Fig 3B, the model highlights a double saline bridge (K_{665} and K_{666} of CNBD with E_{265} and E_{264} of TRIP8b$_{nano}$) in line with the ITC results described above (Appendix Fig S3). Of note, the contribution of residue R_{662} to the binding is also consistent with previous experiments showing residual TRIP8b interaction in a CNBD deletion mutant ending at position 663 (Saponaro *et al*, 2014). Our modelling data suggest that, upon folding of the distal portion of the C-helix, the side chains of residues R_{662} and R_{665} face to the inside when contacting cAMP but face to the outside when binding TRIP8b (Appendix Fig S4).

In addition to clarifying the role of residues in the distal portion of the CNBD C-helix, the model also highlights a second important cluster of electrostatic interactions with R_{650} in the proximal portion of the CNBD C-helix contacting E_{240} and E_{241} in helix N of TRIP8b$_{nano}$ (Fig 3C). To confirm the contribution of these residues, we reversed charges and tested each residue mutation for binding in ITC. The results in Appendix Fig S3 show that $R_{650}E$ caused a more than six-fold reduction in binding affinity for TRIP8b$_{nano}$, with smaller but significant effects seen also for $E_{240}R$ and $E_{241}R$.

A third important contact highlighted by the model is the interaction between N_{547} in the N-bundle loop of the CNBD and D_{252} in the link between helix N and helix C of TRIP8b$_{nano}$ (Fig 3D). We tested this potential interaction by disrupting the expected hydrogen bond between N_{547} and the carboxyl group of the negative residue (D_{252}) in TRIP8b$_{nano}$. The asparagine in CNBD was mutated into aspartate ($N_{547}D$) to generate an electrostatic repulsion for D_{252}, and the carboxyl group in D_{252} of TRIP8b$_{nano}$ was removed by mutation into asparagine

bioRxiv preprint doi: https://doi.org/10.1101/253096; this version posted January 24, 2018. The copyright holder for this preprint (which was not certified by peer review) is the author/funder, who has granted bioRxiv a license to display the preprint in perpetuity. It is made available under aCC-BY-NC-ND 4.0 International license.

($D_{252}N$). As predicted, $N_{547}D$ greatly reduced binding to TRIP8b in ITC assays (Appendix Fig S3), with a smaller but significant effect observed also for $D_{252}N$ (Appendix Fig S3). These results confirm and extend our previous finding that the N-bundle loop contributes in a substantial manner to the binding of TRIP8b (Saponaro *et al*, 2014).

TRIP8b$_{nano}$ as a tool for the direct regulation of native HCN currents

Next, we asked whether the relatively short TRIP8b$_{nano}$ peptide could be used to block the response of HCN channels to cAMP by delivering the peptide to full length channels heterologously expressed in cells. To this end, we dialyzed TRIP8b$_{nano}$ into the cytosol of HEK 293T cells transfected either with HCN1, HCN2, or HCN4 channels. The peptide was added (10 µM) in the recording pipette together with a non-saturating concentration of cAMP for each isoform (5 µM for HCN2, 1 µM for HCN4) expected to produce a ~10 mV rightward shift in the mid-activation potential ($V_{1/2}$) in the wildtype channels (Fig 4). No cAMP was added in the case of HCN1, as this isoform is already fully shifted by low endogenous cAMP levels (Fig 4 and Appendix Fig. S5). The results of the respective recordings in the presence and absence of TRIP8b$_{nano}$ show that the peptide fully abolished the cAMP-induced potentiation of channel opening in all HCN isoforms (Fig 4).

Thus, we reckoned it may be employed as a regulatory tool for native I_f/I_h currents. As proof of principle, we tested whether TRIP8b$_{nano}$ can modulate the frequency of action potential firing in sinoatrial node (SAN) cells. In these cells, I_f contributes substantially to the diastolic depolarization phase of the action potential. Moreover, the autonomic nervous system modulates the frequency of action potential firing by changing intracellular cAMP levels, which in turn acts on HCN channel open probability (DiFrancesco, 1993). The native I_f current from cardiomyocytes acutely isolated from rabbit sinoatrial node (SAN) was recorded with and without 10 µM TRIP8b$_{nano}$ in the pipette solution (Fig 5A). Fig 5B shows that the activation curve recorded in presence of TRIP8b$_{nano}$ is significantly hyperpolarized

bioRxiv preprint doi: https://doi.org/10.1101/253096; this version posted January 24, 2018. The copyright holder for this preprint (which was not certified by peer review) is the author/funder, who has granted bioRxiv a license to display the preprint in perpetuity. It is made available under aCC-BY-NC-ND 4.0 International license.

compared to the control. This indicates that the peptide is displacing the binding of endogenous cAMP to native HCN channels. Moreover, when the experiment was repeated in the presence of 1 µM cAMP, TRIP8b$_{nano}$ prevented the typical cAMP-dependent potentiation of the native I_f current (Fig 5B). In light of these results, we tested whether TRIP8b$_{nano}$ is also able to modulate cardiac automaticity by antagonizing basal cAMP. The data in Fig 5C show that TRIP8b$_{nano}$ indeed significantly decreased the rate of action potential firing in single SAN cells. Strikingly, the observed 30% decrease in action potential rate corresponds to the effect induced by physiological concentrations of acetylcholine (DiFrancesco *et al*, 1989).

To conclusively prove that the inhibition of the native I_f current was specifically due to TRIP8b$_{nano}$ rather than caused by the dilution of the cellular content followed by whole cell configuration, we created a TAT version of TRIP8b$_{nano}$ (hereafter TAT-TRIP8b$_{nano}$). Indeed, TAT sequence allows the entry of biomolecules into a cell via endocytosis, thus leaving unaltered the cytosolic content (Guidotti *et al*, 2017).

We thus tested whether both TRIP8b$_{nano}$ and TAT-TRIP8b$_{nano}$ were able to selectively inhibit the beta-adrenergic stimulation of I_f current, while leaving unaltered the potentiation of L-type Ca^{2+} current ($I_{Ca,L}$). To this end, we recorded either the native I_f or $I_{Ca,L}$ current from cardiomyocytes acutely isolated from mouse sinoatrial node (SAN) in the presence and in the absence of 10 µM TRIP8b$_{nano}$ or TAT-TRIP8b$_{nano}$, before and after stimulation with 100 nM isoproterenol, a β-adrenergic receptor agonist (Fig 6). Strikingly, TRIP8b$_{nano}$ prevented the isoproterenol-induced increase of I_f current density, both when the peptide was added in the recording pipette solution (Fig 6A and 6B), and when it was used in the TAT version (Fig 6A and 6C). The specificity of TRIP8b$_{nano}$ for I_f current was confirmed by the absence inhibition of the I_{Ca},L current (fig 6D). Indeed, we failed to record a significant difference in

bioRxiv preprint doi: https://doi.org/10.1101/253096; this version posted January 24, 2018. The copyright holder for this preprint (which was not certified by peer review) is the author/funder, who has granted bioRxiv a license to display the preprint in perpetuity. It is made available under aCC-BY-NC-ND 4.0 International license.

the isoproterenol-stimulated increase of the I_{Ca},L current density between the control condition and 10µM TRIP8b$_{nano}$ (fig 6E) or TAT-TRIP8b$_{nano}$ (fig 6F) conditions.

Discussion

TRIP8b-CNBD complex

In the present study, we describe the interaction between TRIP8b and the HCN channel CNBD at atomic level, based on a NMR-derived structural model of their complex. The data show that the minimal binding unit of TRIP8b, TRIP8b$_{nano}$, folds in two helices upon binding, suggesting that this region of the regulatory subunit has an intrinsically disordered behavior when not in the complex. The model structurally validates previous indirect evidence, which suggested that TRIP8b binds to two different elements of the CNBD, the N-bundle loop and the C-helix. As a consequence of the interaction with TRIP8b$_{nano}$, the C-helix in the CNBD increases in length, a behavior already observed in the case of cAMP binding. The model also identifies residues R_{662} and K_{665} in the CNBD as interaction partners with TRIP8b$_{nano}$, two cationic residues also involved in cAMP binding (Zhou & Siegelbaum, 2007). The finding that TRIP8b and cAMP share binding sites on the C-helix provides a solid molecular explanation for functional data which underscore a competition between the two regulators (Han *et al*, 2011; Deberg *et al*, 2015; Bankston *et al*, 2017). However, it has been previously suggested that a direct competition model does not fully explain the mutually antagonistic effect of the two ligands (Hu *et al*, 2013). Specifically, the fact that the inhibitory effect of TRIP8b on channel activity persists even at saturating cAMP concentrations suggests an allosteric component in the regulation mechanism. Our structural model provides the missing molecular evidence for this allosteric component. TRIP8b$_{nano}$ binds to the solvent-exposed elements of CNBD (N-bundle loop and C-helix) and does not interact directly with the buried PBC, which remains unfolded, as demonstrated by the observation that the P-

bioRxiv preprint doi: https://doi.org/10.1101/253096; this version posted January 24, 2018. The copyright holder for this preprint (which was not certified by peer review) is the author/funder, who has granted bioRxiv a license to display the preprint in perpetuity. It is made available under aCC-BY-NC-ND 4.0 International license.

helix does not form upon TRIP8b binding. This rules out the possibility that TRIP8b$_{nano}$ controls the affinity for cAMP by directly binding to the PBC. Rather, it confirms that the PBC in the complex is indirectly kept in the low affinity state for cAMP binding (unfolded form) through allosteric long-range interactions.

TRIP8b$_{nano}$ as a tool for modulating native I_f currents

TRIP8b$_{nano}$ is a minimal protein fragment, which binds the HCN channel CNBD with high affinity and fully abolishes the cAMP effect in all tested isoforms (HCN1, 2 and 4). Given the small size of the peptide (<5kD), TRIP8b$_{nano}$ may be easily adapted for *in vivo* delivery, and thus constitutes a promising tool for the study or modulation of native HCN channels in systems where the regulatory protein is not expressed, or is expressed at low levels. To this end, we successfully fused to TRIP8b$_{nano}$ an internalization sequence that delivered the peptide into sinoatrial node myocytes via the physiological pathway of the endocytosis without affecting TRIP8b$_{nano}$ function. This modification may significantly expand the use of TRIP8b$_{nano}$ as a tool for non-invasive and *in vivo* functional assays.

Our structural model explains why a previous attempt at identifying the minimal domain required for TRIP8b activity resulted in a peptide with strongly reduced CNDB affinity, as the fragment selected in the study by Lyman et al (Lyman *et al*, 2017) is lacking an important contact residue (E_{240}). In the present study, we successfully used TRIP8b$_{nano}$ to selectively control native I_f currents and pacemaking in sinoatrial node cardiomyocytes. Unlike channel blockers, which inhibit ionic currents, the peptide only interferes with the cAMP-based regulation of HCN channels, while leaving basal HCN functions unaltered. In addition, and in contrast to even the most selective blockers, it is entirely specific for HCN channels. The ability to selectively control a specific molecular mechanism to modulate channel activity represents a novel approach, which yields the promise of a more targeted therapeutic intervention compared to pore blockers.

bioRxiv preprint doi: https://doi.org/10.1101/253096; this version posted January 24, 2018. The copyright holder for this preprint (which was not certified by peer review) is the author/funder, who has granted bioRxiv a license to display the preprint in perpetuity. It is made available under aCC-BY-NC-ND 4.0 International license.

Materials and Methods

Constructs

The cDNA fragment encoding residues 235 – 275 (TRIP8b$_{nano}$) of mouse TRIP8b (splice variant 1a4) was cloned into pET-52b (EMD Millipore) downstream of a Strep (II) tag sequence, while the cDNA fragment encoding residues 521–672 of human HCN2 (HCN2 CNBD) was cloned, in a previous study, into a modified pET-24b downstream of a double His$_6$-maltose-binding protein (MBP) (Saponaro *et al*, 2014). The cDNA encoding full-length human HCN1 channel, mouse HCN2 channel, rabbit HCN4 channel and mouse TRIP8b (1a4) were cloned into the eukaryotic expression vector pcDNA 3.1 (Clontech Laboratories). Mutations were generated by site-directed mutagenesis (QuikChange site-directed mutagenesis kit; Agilent Technologies) and confirmed by sequencing.

Preparation of proteins

The HCN2 CNBD WT and mutant proteins, as well as the TRIP8b$_{core}$ and TRIP8b$_{nano}$ proteins (WT and mutants) were produced and purified following the procedure previously described (Saponaro *et al*, 2014).

Structure calculation of the cAMP-free human HCN2 CNBD in complex with TRIP8b$_{nano}$ and vice versa

NMR experiments were acquired on Bruker Avance III 950, 700 and 500 MHz NMR spectrometers equipped with a TXI-cryoprobe at 298 K. The acquired triple resonance NMR experiments for the assignment of backbone resonances of cAMP-free HCN2 CNBD (CNBD hereafter) in complex with TRIP8b$_{nano}$ and vice versa are summarized in Table S1. ^{15}N, $^{13}C'$, $^{13}C_\alpha$, $^{13}C_\beta$, and H_α chemical shifts were used to derive ϕ and ψ dihedral angles by TALOS+ program (Cornilescu *et al*, 1999) for both CNBD and TRIP8b$_{nano}$. For TRIP8b$_{nano}$, CYANA-2.1 structure calculation (Guntert & Buchner, 2015) was performed using 68 ϕ and ψ dihedral angles and 40 backbone hydrogen bonds as input. For CNBD, CYANA-2.1 structure calculation was performed using 108 ϕ and ψ dihedral angles, combined with the NOEs obtained in our previous determination of the cAMP-free form of the CNBD (Saponaro *et al*, 2014) for those regions not affected by the interaction with TRIP8b$_{nano}$. The 10 conformers of TRIP8b$_{nano}$ and CNBD with the lowest residual target function values were subjected to restrained energy minimization with AMBER 12.0 (Santoro *et al*, 2011)

bioRxiv preprint doi: https://doi.org/10.1101/253096; this version posted January 24, 2018. The copyright holder for this preprint (which was not certified by peer review) is the author/funder, who has granted bioRxiv a license to display the preprint in perpetuity. It is made available under aCC-BY-NC-ND 4.0 International license.

(http://pyenmr.cerm.unifi.it/access/index/amps-nmr) and used as input in docking calculations.

Docking calculations

Docking calculations were performed with HADDOCK2.2 implemented in the WeNMR/West-Life GRID-enabled web portal (www.wenmr.eu). The docking calculations are driven by ambiguous interaction restraints (AIRs) between all residues involved in the intermolecular interactions (Dominguez *et al*, 2003). Active residues of the CNBD were defined as the surface exposed residues (at least 50% of solvent accessibility), which show chemical shift perturbation upon TRIP8b$_{nano}$ binding.

The assignment of the CNBD bound to TRIP8b$_{nano}$ allowed to highlight the residues of CNBD whose backbone featured appreciable Combined Chemical Shift Perturbation (CSP) (Fig S1). The combined CSP (Δ_{HN}) is given by the equation $\Delta_{HN}=\{((H_{Nfree}-H_{Nbound})^2+((N_{free}-N_{bound})/5)^2)/2\}^{½}$ (Garrett *et al*, 1997).

Passive residues of CNBD were defined as the residues close in space to active residues and with at least 50% solvent accessibility.

In the case of TRIP8b$_{nano}$, the conserved stretch E_{239}-E_{243}, located in helix N, was defined as active region in a first docking calculation, while all the other solvent accessible residues of the peptide were defined as passive. This docking calculation generated several clusters. A post-docking filter step allowed us to select those clusters having an orientation of TRIP8b$_{nano}$ bound to CNBD in agreement with a DEER study on the CNBD - TRIP8b$_{nano}$ interaction (Deberg *et al*, 2015). The selected clusters grouped in two classes on the basis of the orientation of helix N of TRIP8b$_{nano}$ (N) relative to CNBD (Fig S2). A second docking calculation was subsequently performed introducing also residues E_{264}-E_{265}, located in helix C of TRIP8b$_{nano}$ as active residues. The active residues for CNBD were the same used for the first calculation. For this second HADDOCK calculation 14 clusters were obtained and ranked according to their HADDOCK score. Among them only four clusters showed both an orientation of TRIP8b$_{nano}$ bound to CNBD in agreement with the DEER study (Deberg *et al*, 2015) and the involvement of E_{239}-E_{243} stretch of TRIP8b$_{nano}$ in the binding to CNBD. These clusters were manually analyzed and subjected to a per-cluster re-analysis following the protocol reported in http://www.bonvinlab.org/software/haddock2.2/analysis/#reanal. From this analysis, it resulted that the top-ranking cluster, i.e. the one with the best energetic and scoring functions, has a conformation in agreement with mutagenesis experiments (Fig S3).

bioRxiv preprint doi: https://doi.org/10.1101/253096; this version posted January 24, 2018. The copyright holder for this preprint (which was not certified by peer review) is the author/funder, who has granted bioRxiv a license to display the preprint in perpetuity. It is made available under aCC-BY-NC-ND 4.0 International license.

Energy parameters (van der Waals energy, electrostatic energy, desolvation energy, and the penalty energy due to violation of restraints) for this complex model are reported in Table S2.

Both docking calculations were performed using 10 NMR conformers of both the CNBD and the TRIP8b$_{nano}$ structures calculated as described above. In the TRIP8b$_{nano}$ structures the unfolded N- and C-terminal regions were removed, while in the CNBD structures only the unfolded N-terminal region was removed. This is because the C-terminal region of the CNBD is known to comprise residues involved in TRIP8b$_{nano}$ binding (Saponaro *et al*, 2014). Flexible regions of the proteins were defined based on the active and passive residues plus two preceding and following residues. The residue solvent accessibility was calculated with the program NACCESS (Hu *et al*, 2013). In the initial rigid body docking calculation phase, 5000 structures of the complex were generated, and the best 400 in terms of total intermolecular energy were further submitted to the semi-flexible simulated annealing and a final refinement in water. Random removal of the restraints was turned off. The number of flexible refinement steps was increased from the default value of 500/500/1000/1000 to 2000/2000/2000/4000. The final 400 structures were then clustered using a cutoff of 5.0 Å of RMSD to take into consideration the smaller size of protein-peptide interface.

Electrophysiology of HEK 293T cells

HEK 293T cells were cultured in Dulbecco's modified Eagle's medium (Euroclone) supplemented with 10% fetal bovine serum (Euroclone), 1% Pen Strep (100 U/mL of penicillin and 100 µg/ml of streptomycin), and stored in a 37°C humidified incubator with 5% CO_2. The plasmid containing cDNA of wild-type and mutant HCN1, HCN2 and HCN4 channels (1 µg) was co-transfected for transient expression into HEK 293T cells with a plasmid containing cDNA of Green Fluorescent Protein (GFP) (1.3 µg). For co-expression with TRIP8b (1a-4), HEK 293T cells were transiently transfected with wild-type (wt) and/or mutant human HCN1 cDNA (1 µg), wt TRIP8b (1a-4) cDNA (1 µg) and cDNA of Green Fluorescent Protein (GFP) (0.3 µg).

One day after transfection, GFP-expressing cells were selected for patch-clamp experiments in whole-cell configuration. The experiments were conducted at R.T. The pipette solution in whole cell experiments contained: 10 mM NaCl, 130 mM KCl, 1 mM egtazic acid (EGTA), 0.5 mM $MgCl_2$, 2 mM ATP (Mg salt) and 5 mM HEPES–KOH buffer (pH 7.4). The extracellular bath solution contained 110 mM NaCl, 30 mM KCl, 1.8 mM $CaCl_2$, 0.5 mM $MgCl_2$ and 5 mM HEPES–KOH buffer (pH 7.4).

bioRxiv preprint doi: https://doi.org/10.1101/253096; this version posted January 24, 2018. The copyright holder for this preprint (which was not certified by peer review) is the author/funder, who has granted bioRxiv a license to display the preprint in perpetuity. It is made available under aCC-BY-NC-ND 4.0 International license.

TRIP8b$_{nano}$ was added (10 μM) to the pipette solution. cAMP was added at different concentration to the pipette solution depending on the HCN isoform used: 0 μM for HCN1, 5 μM for HCN2 and 1 μM for HCN4.

Whole-cell measurements of HCN channels were performed using the following voltage clamp protocol depending on the HCN isoform measured: for HCN1, holding potential was –30 mV (1s), with steps from –40 mV to –130 mV (10 mV interval, 3.5 s) and tail currents recorded at –40mV (3 s); for HCN2, holding potential was –30 mV (1 s), with steps from –40 mV to –150 mV (10 mV interval, 5 s) and tail currents recorded at -40mV (5 s); for HCN4, holding potential was –30 mV (1s), steps from –40 mV to –160 mV (10 mV interval, 6 s) and tail currents were recorded at -40mV (6 s).

Isolation and electrophysiology of rabbit sinoatrial node cells

Animal protocols conformed to the guidelines of the care and use of laboratory animals established by Italian and European Directives (D. Lgs n° 2014/26, 2010/63/UE). New Zealand white female rabbits (0.8–1.2 kg) were anesthetized (xylazine 5mg/Kg, i.m.), and euthanized with an overdose of sodium thiopental (i.v.); hearts were quickly removed, and the SAN region was isolated and cut in small pieces. Single SAN cardiomyocytes were isolated following an enzymatic and mechanical procedure as previously described (DiFrancesco *et al*, 1986). Following isolation, cells were maintained at 4 °C in Tyrode solution: 140 mM NaCl, 5.4 mM KCl, 1.8 mM $CaCl_2$, 1 mM $MgCl_2$, 5.5 mM D-glucose, 5 mM HEPES-NaOH (pH 7.4).

For patch clamp experiments cells were placed in a chamber on an inverted microscope and experiments were performed in the whole-cell configuration at 35 ± 0.5 °C. The pipette solution contained: 10 mM NaCl, 130 mM KCl, 1 mM egtazic acid (EGTA), 0.5 mM $MgCl_2$, and 5 mM HEPES–KOH buffer (pH 7.2). The I_f current was recorded from single cells superfused with Tyrode solution with 1 mM $BaCl_2$, and 2 mM $MnCl_2$.

I_f activation curves were obtained using a two-step protocol in which test voltage steps (from -30 to -120 mV, 15 mV interval) were applied from a holding potential of -30 mV and were followed by a step to -125 mV. Test steps had variable durations so as to reach steady – state activation at all voltages.

In current-clamp studies, spontaneous action potentials were recorded from single cells superfused with Tyrode solution, and rate was measured from the interval between

bioRxiv preprint doi: https://doi.org/10.1101/253096; this version posted January 24, 2018. The copyright holder for this preprint (which was not certified by peer review) is the author/funder, who has granted bioRxiv a license to display the preprint in perpetuity. It is made available under aCC-BY-NC-ND 4.0 International license.

successive action potential. When indicated cAMP (1 µM) and/or nanoTRIP8b (10 µM) were added to the pipette solution.

Isolation and electrophysiology of mouse sinoatrial node cells

Mice were killed by cervical dislocation under general anesthesia consisting of 0.01 mg/g xylazine (2% Rompun; Bayer AG), 0.1 mg/g ketamine (Imalgène; Merial) and 0.04mg/g of Na-pentobarbital (Euthanasol VET, Laboratoire TVM, Lempdes, France), and beating hearts were quickly removed. The SAN region was excised in warmed (35°C) Tyrode's solution containing: 140 mM NaCl, 5.4 mM KCl, 1.8 mM $CaCl_2$, 1 mM $MgCl_2$, 1 mM Hepes-NaOH (pH = 7.4), and 5.5 mM D-glucose and cut in strips. Strips were then transferred into a "low-Ca^{2+}-low-Mg^{2+}" solution containing: 140 mM NaCl; 5.4 mM KCl, 0.5 mM $MgCl_2$, 0.2 mM $CaCl_2$, 1.2 mM KH_2PO_4, 50 mM taurine, 5.5 mM D-glucose, 1 mg/ml bovine serum albumin (BSA), 5 mM Hepes-NaOH (pH = 6.9).

Tissue was digested by adding Liberase TH (0.15 mg/ml, Roche Diagnostics GmbH, Mannheim, Germany), elastase (1.9 U/ml, Worthington, Lakewood, USA). Digestion was carried out for a variable time of 15–18 minutes at 35°C. Tissue strips were then washed and transferred into a modified "Kraftbrühe" (KB) medium containing: 70 mM L-glutamic acid, 20 mM KCl, 80 mM KOH, (±) 10 mM D- b-OH-butyric acid; 10 mM KH_2PO_4, 10 mM taurine, 1mg/ml BSA and 10 mM Hepes-KOH (pH = 7.4).

Single SAN cells were isolated by manual agitation in KB solution at 35°C for 30–50 seconds.

Cellular automaticity was recovered by re-adapting the cells to a physiological extracellular Ca^{2+} concentration by addition of a solution containing: 10 mM NaCl, 1.8 mM $CaCl_2$ and normal Tyrode solution containing BSA (1 mg/ml). The final storage solution contained: 100 mM NaCl, 35 mM KCl, 1.3 mM $CaCl_2$, 0.7 mM $MgCl_2$, 14 mM L-glutamic acid, (±) 2 mM D-b-OH-butyric acid, 2 mM KH_2PO_4, 2 mM taurine, 1 mg/ml BSA, (pH = 7.4). Cells were then stored at room temperature until use. All chemicals were from SIGMA (St Quentin Fallavier, France).

For electrophysiological recording, SAN cells in the storage solution were harvested in special custom-made recording plexiglas chambers with glass bottoms for proper cell attachment and mounted on the stage of an inverted microscope (Olympus IX71) and perfused with normal Tyrode solution. The recording temperature was 36°C. We used the whole-cell variation of the patch-clamp technique to record cellular ionic currents, by

bioRxiv preprint doi: https://doi.org/10.1101/253096; this version posted January 24, 2018. The copyright holder for this preprint (which was not certified by peer review) is the author/funder, who has granted bioRxiv a license to display the preprint in perpetuity. It is made available under aCC-BY-NC-ND 4.0 International license.

employing a Multiclamp 700B (Axon Instruments Inc., Foster USA) patch clamp amplifier. Recording electrodes were fabricated from borosilicate glass, by employing a WZ DMZ-Universal microelectrode puller (Zeitz-Instruments Vertriebs GmbH, Martinsried, Germany).

If was recorded under standard whole-cell configuration during perfusion of standard Tyrode's containing 2 mM $BaCl_2$ to block I_{K1}. Patch-clamp pipettes were filled with an intracellular solution containing: 130 mM KCl, 10 mM NaCl, 1 mM EGTA, 0.5 mM $MgCl_2$ and 5 mM HEPES (pH 7.2).

For recording of L-type calcium currents, pipette solution contained: 125 mM CsOH, 20 mM tetraethylammonium chloride (TEA-Cl), 1.2 mM $CaCl_2$, 5 mM Mg-ATP, 0.1 mM Li_2-GTP, 5 mM EGTA and 10 mM HEPES (pH 7.2 with aspartate). 30 µM TTX (Latoxan, Portes lès Valence, France) to block INa was added to external solution containing: 135 mM tetraethylammonium chloride (TEA-Cl), 4 mM $CaCl_2$,10 mM 4-amino-pyridine, 1 mM $MgCl_2$, 10 mM HEPES and 1 mg/ml Glucose (pH 7.4 with TEA-OH).

Electrodes had a resistance of about 3 MΩ. Seal resistances were in the range of 2–5 GΩ.

10µM TRIPb8$_{nano}$ was added to pipette solution. 10µM TAT-TRIPb8$_{nano}$ was added in cell storage solution for at least 30 min before patch clamp recording.

Data analysis

Data were acquired at 1 kHz using an Axopatch 200B amplifier and pClamp10.5 software (Axon Instruments). Data were analyzed off-line using Clampfit 10.5 (Molecular Devices) and Origin 16 (OriginLab Corp., Northampton MA). Activation curves were analyzed by the Boltzmann equation, $y=1/\{1+\exp[(V-V1/2)/s]\}$, where y is fractional activation, V is voltage, $V_{1/2}$ half-activation voltage, and s the inverse slope factor (mV) (DiFrancesco, 1999). Mean activation curves were obtained by fitting individual curves from each cell to the Boltzmann equation and then averaging all curves obtained.

ACKNOWLEDGEMENTS

This work has been supported by Fondazione CARIPLO grant 2014-0796 to A.M., B.S and L.B. and partly by 2016 Schaefer Research Scholars Program of Columbia University to A.M., by MIUR PRIN (Programmi di Ricerca di Rilevante Interesse Nazionale) 494 2015

bioRxiv preprint doi: https://doi.org/10.1101/253096; this version posted January 24, 2018. The copyright holder for this preprint (which was not certified by peer review) is the author/funder, who has granted bioRxiv a license to display the preprint in perpetuity. It is made available under aCC-BY-NC-ND 4.0 International license.

(2015795S5W) to A.M., by European Research Council (ERC) 2015 Advanced Grant 495 (AdG) n. 695078 noMAGIC to A.M. and G.T., by National Institutes for Health Grant R01 NS036658 to B.S., by Instruct-ERIC and national member subscriptions to L.B., by Accademia Nazionale dei Lincei (Giuseppe Levi foundation) to A.S. We specially thank the EU ESFRI Instruct Core Centre CERM-Italy.

Author contributions

A.S. designed and prepared constructs, performed biochemical experiments and analyzed the data, C.D. and B.I. designed constructs and purified proteins, F.C. and V.M. performed the NMR measurements and analyzed the data, A.P. performed the patch measurements in HEK293T cells, D.D.F. and A.B. designed the expriments and A.B: performed the measurements in rabbit SAN myocytes, M.M. and P.M. designed the experiments and P.M. performed the measurements in mouse SAN myocytes. L.B., B.S., G.T. and A.M. conceived the study and wrote the manuscript. A.M. coordinated the research team.

Conflict of interest: none

References

Bankston JR, DeBerg HA, Stoll S & Zagotta WN (2017) Mechanism for the inhibition of the cAMP dependence of HCN ion channels by the auxiliary subunit TRIP8b. *J. Biol. Chem.*

Cornilescu G, Delaglio F & Bax A (1999) Protein backbone angle restraints from searching a database for chemical shift and sequence homology. *J. Biomol. NMR* **13:** 289–302

Deberg HA, Bankston JR, Rosenbaum JC, Brzovic PS, Zagotta WN & Stoll S (2015) Structural mechanism for the regulation of HCN ion channels by the accessory protein TRIP8b. *Structure* **23:** 734–744

DiFrancesco D (1993) Pacemaker mechanisms in cardiac tissue. *Annu. Rev. Physiol.* **55:** 455–472

DiFrancesco D (1999) Dual allosteric modulation of pacemaker (f) channels by cAMP and voltage in rabbit SA node. *J. Physiol.* **515 (Pt 2:** 367–376

DiFrancesco D, Ducouret P & Robinson RB (1989) Muscarinic modulation of cardiac rate at low acetylcholine concentrations. *Science (80-.).* **243:** 669–671 Available at: http://www.ncbi.nlm.nih.gov/pubmed/2916119

DiFrancesco D, Ferroni A, Mazzanti M & Tromba C (1986) Properties of the hyperpolarizing-activated current (if) in cells isolated from the rabbit sino-atrial node. *J. Physiol.* **377:** 61–88

bioRxiv preprint doi: https://doi.org/10.1101/253096; this version posted January 24, 2018. The copyright holder for this preprint (which was not certified by peer review) is the author/funder, who has granted bioRxiv a license to display the preprint in perpetuity. It is made available under aCC-BY-NC-ND 4.0 International license.

Dominguez C, Boelens R & Bonvin AMJJ (2003) HADDOCK: a protein-protein docking approach based on biochemical or biophysical information. *J. Am. Chem. Soc.* **125:** 1731–1737

Dyson HJ & Wright PE (2004) Unfolded proteins and protein folding studied by NMR. *Chem. Rev.* **104:** 3607–3622

Garrett DS, Seok YJ, Peterkofsky A, Clore GM & Gronenborn AM (1997) Identification by NMR of the binding surface for the histidine-containing phosphocarrier protein HPr on the N-terminal domain of enzyme I of the Escherichia coli phosphotransferase system. *Biochemistry* **36:** 4393–4398

Guidotti G, Brambilla L & Rossi D (2017) Cell-Penetrating Peptides: From Basic Research to Clinics. *Trends Pharmacol. Sci.* **38:** 406–424

Guntert P & Buchner L (2015) Combined automated NOE assignment and structure calculation with CYANA. *J. Biomol. NMR* **62:** 453–471

Han Y, Noam Y, Lewis AS, Gallagher JJ, Wadman WJ, Baram TZ & Chetkovich DM (2011) Trafficking and gating of hyperpolarization-activated cyclic nucleotide-gated channels are regulated by interaction with tetratricopeptide repeat-containing Rab8b-interacting protein (TRIP8b) and cyclic AMP at distinct sites. *J. Biol. Chem.* **286:** 20823–20834

Hu L, Santoro B, Saponaro A, Liu H, Moroni A & Siegelbaum S (2013) Binding of the auxiliary subunit TRIP8b to HCN channels shifts the mode of action of cAMP. *J. Gen. Physiol.* **142:** 599–612 Available at: http://www.jgp.org/lookup/doi/10.1085/jgp.201311013

Lee C-H & MacKinnon R (2017) Structures of the Human HCN1 Hyperpolarization-Activated Channel. *Cell* **168:** 111–120.e11

Lewis AS, Schwartz E, Chan CS, Noam Y, Shin M, Wadman WJ, Surmeier DJ, Baram TZ, Macdonald RL & Chetkovich DM (2009) Alternatively spliced isoforms of TRIP8b differentially control h channel trafficking and function. *J. Neurosci.* **29:** 6250–6265

Lyman KA, Han Y, Heuermann RJ, Cheng X, Kurz JE, Lyman RE, Van Veldhoven PP & Chetkovich DM (2017) Allostery between two binding sites in the ion channel subunit TRIP8b confers binding specificity to HCN channels. *J. Biol. Chem.*

Piskorowski R, Santoro B & Siegelbaum SA (2011) TRIP8b Splice Forms Act in Concert to Regulate the Localization and Expression of HCN1 Channels in CA1 Pyramidal Neurons. *Neuron* **70:** 495–509

Puljung MC & Zagotta WN (2013) A secondary structural transition in the C-helix promotes gating of cyclic nucleotide-regulated ion channels. *J. Biol. Chem.* **288:** 12944–12956

Robinson RB & Siegelbaum SA (2003) Hyperpolarization-Activated Cation Currents: From Molecules to Physiological Function. *Annu. Rev. Physiol.* **65:** 453–480 Available at: http://www.annualreviews.org/doi/10.1146/annurev.physiol.65.092101.142734

Santoro B, Hu L, Liu H, Saponaro A, Pian P, Piskorowski RA, Moroni A & Siegelbaum SA (2011) TRIP8b Regulates HCN1 Channel Trafficking and Gating through Two Distinct C-Terminal Interaction Sites. *J. Neurosci.* **31:** 4074–4086 Available at: http://www.jneurosci.org/cgi/doi/10.1523/JNEUROSCI.5707-10.2011

Santoro B, Piskorowski RA, Pian P, Hu L, Liu H & Siegelbaum SA (2009) TRIP8b Splice Variants Form a Family of Auxiliary Subunits that Regulate Gating and Trafficking of HCN Channels in the Brain. *Neuron* **62:** 802–813

Saponaro A, Pauleta SR, Cantini F, Matzapetakis M, Hammann C, Donadoni C, Hu L, Thiel G, Banci L, Santoro B & Moroni A (2014) Structural basis for the mutual antagonism of cAMP and TRIP8b in regulating HCN channel function. *Proc. Natl. Acad. Sci. U. S. A.* **111:** 14577–14582

bioRxiv preprint doi: https://doi.org/10.1101/253096; this version posted January 24, 2018. The copyright holder for this preprint (which was not certified by peer review) is the author/funder, who has granted bioRxiv a license to display the preprint in perpetuity. It is made available under aCC-BY-NC-ND 4.0 International license.

Wainger BJ, DeGennaro M, Santoro B, Siegelbaum SA & Tibbs GR (2001) Molecular mechanism of cAMP modulation of HCN pacemaker channels. *Nature* **411:** 805–810 Available at: http://www.nature.com/doifinder/10.1038/35081088

Zagotta WN, Olivier NB, Black KD, Young EC, Olson R & Gouaux E (2003) Structural basis for modulation and agonist specificity of HCN pacemaker channels. *Nature* **425:** 200–205 Available at: http://www.nature.com/doifinder/10.1038/nature01922

Zhou L & Siegelbaum SA (2007) Gating of HCN channels by cyclic nucleotides: residue contacts that underlie ligand binding, selectivity, and efficacy. *Structure* **15:** 655–670

Zolles G, Wenzel D, Bildl W, Schulte U, Hofmann A, Muller CS, Thumfart J-O, Vlachos A, Deller T, Pfeifer A, Fleischmann BK, Roeper J, Fakler B & Klocker N (2009) Association with the auxiliary subunit PEX5R/Trip8b controls responsiveness of HCN channels to cAMP and adrenergic stimulation. *Neuron* **62:** 814–825

bioRxiv preprint doi: https://doi.org/10.1101/253096; this version posted January 24, 2018. The copyright holder for this preprint (which was not certified by peer review) is the author/funder, who has granted bioRxiv a license to display the preprint in perpetuity. It is made available under aCC-BY-NC-ND 4.0 International license.

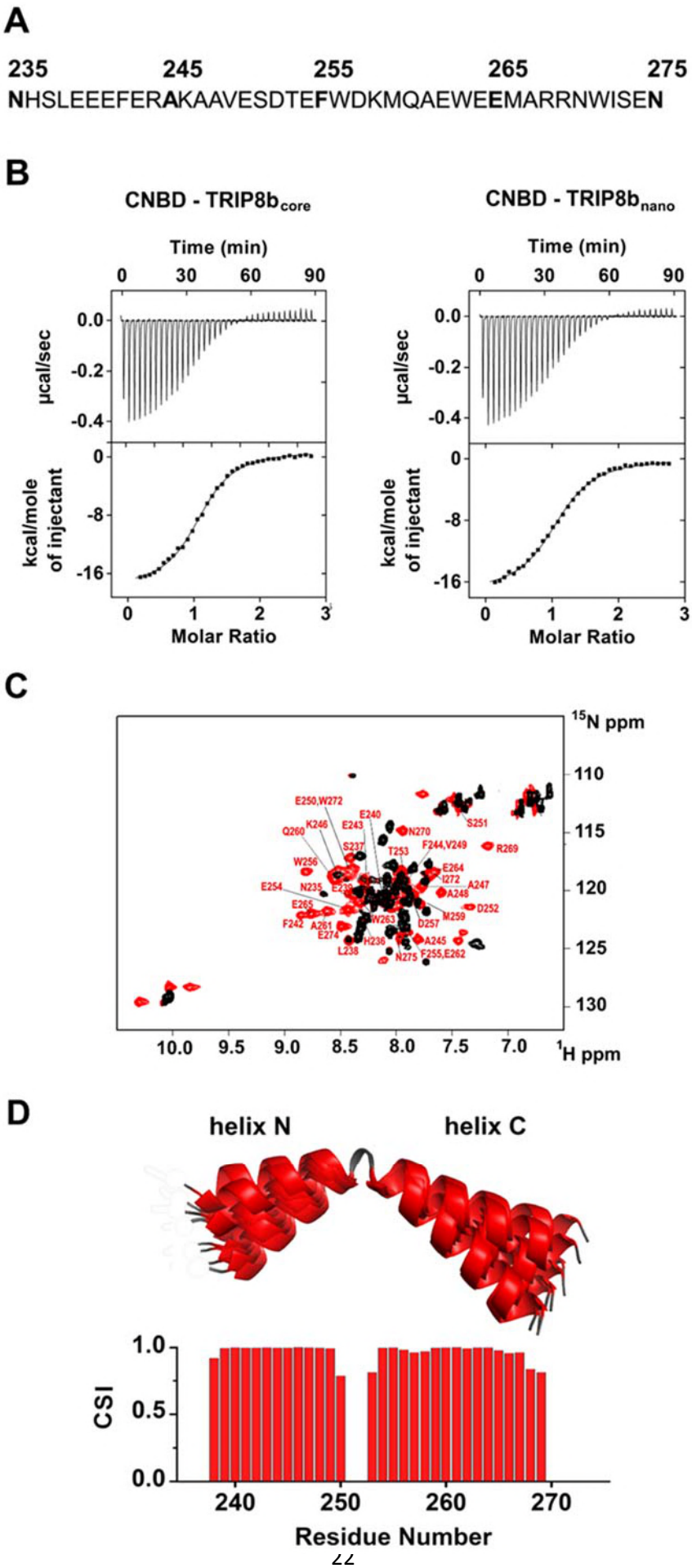

bioRxiv preprint doi: https://doi.org/10.1101/253096; this version posted January 24, 2018. The copyright holder for this preprint (which was not certified by peer review) is the author/funder, who has granted bioRxiv a license to display the preprint in perpetuity. It is made available under aCC-BY-NC-ND 4.0 International license.

Figure 1. Functional and structural characterization of TRIP8b$_{nano}$.

A Primary sequence of TRIP8b$_{nano}$. Amino acid numbering refers to full length mouse TRIP8b (1a4).

B Binding of TRIP8b$_{core}$ and TRIP8b$_{nano}$ to purified His$_6$-MBP-CNBD measured by Isothermal titration calorimetry (ITC). Upper panel, heat changes (µcal/sec) during successive injections of 8 µL of the corresponding TRIP8b peptide (200 µM) into the chamber containing His$_6$-MBP-CNBD (20 µM). Lower panel, binding curve obtained from data displayed in the upper panel. The peaks were integrated, normalized to TRIP8b peptide concentration, and plotted against the molar ratio (TRIP8b peptide / His$_6$-MBP-CNBD). Solid line represents a nonlinear least-squares fit to a single-site binding model, yielding, in the present examples, a K_D = 1.2 ± 0.1 µM for TRIP8b$_{core}$ and K_D = 1.4 ± 0.1 µM for TRIP8b$_{nano}$.

C Evidence for TRIP8b$_{nano}$ folding upon CNBD binding based on the superimposition of the [^{1}H, ^{15}N] heteronuclear single quantum coherence (HSQC) NMR spectrum of CNBD-free TRIP8b$_{nano}$ (black) and CNBD-bound TRIP8b$_{nano}$ (red). The latter experiment was performed at the molar ratio ([CNBD]/[TRIP8b$_{nano}$]) = 3. The backbone amide (HN) signals of the residues of CNBD-bound TRIP8b$_{nano}$ are labelled in red.

D (Top) Ribbon representation of the 10 lowest energy conformers of TRIP8b$_{nano}$ bound to CNBD used for *in silico* modelling of CNBD-TRIP8b$_{nano}$ complex. The unfolded regions at the N- and C-termini of the construct (residues 235–237 and 270 – 275) are omitted for clarity. (Bottom) Chemical Shift Index (CSI, calculated using TALOS+) plotted as a function of the residue number of TRIP8b$_{nano}$ bound to CNBD. Positive values represent helical propensity.

bioRxiv preprint doi: https://doi.org/10.1101/253096; this version posted January 24, 2018. The copyright holder for this preprint (which was not certified by peer review) is the author/funder, who has granted bioRxiv a license to display the preprint in perpetuity. It is made available under aCC-BY-NC-ND 4.0 International license.

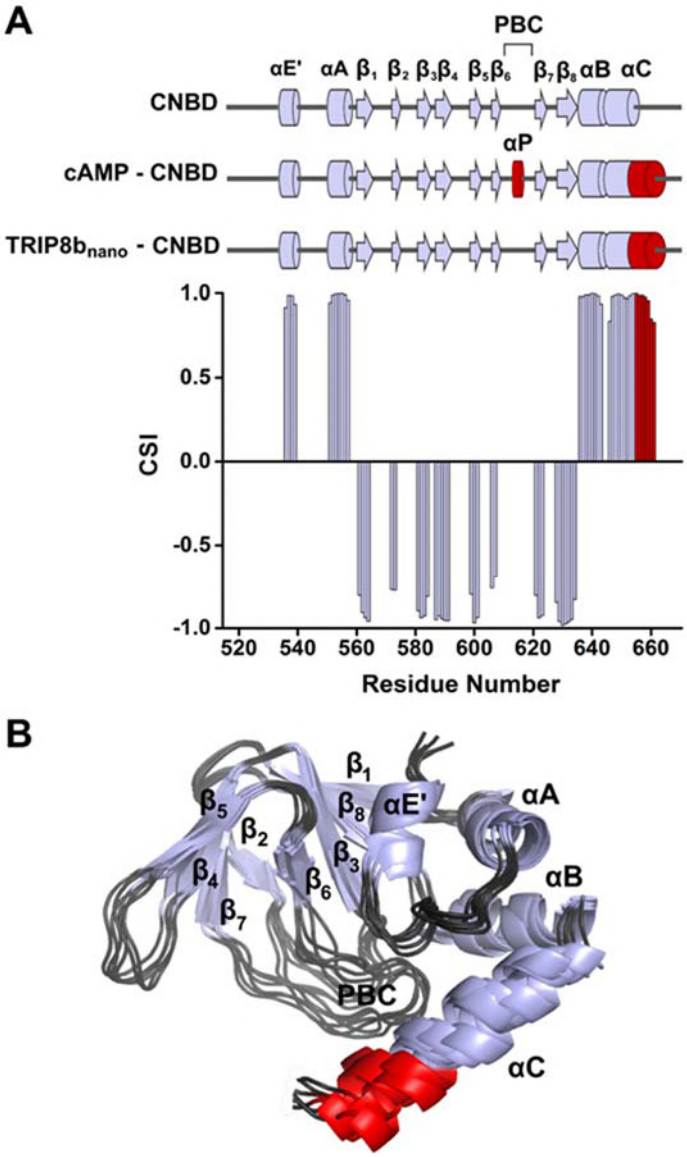

Figure 2. NMR structure of CNBD bound to TRIP8b$_{nano}$.

A (Top) comparison of secondary structure elements of cAMP-free CNBD (Saponaro *et al*, 2014), cAMP-bound CNBD (Zagotta *et al*, 2003) and cAMP-free CNBD bound to TRIP8b$_{nano}$ (this study). Secondary structure elements are indicated by arrows (β-strands) and cylinders (α-helices) and labelled. The loop between β$_6$ and β$_7$ constitutes the Phosphate Binding Cassette (PBC). The elements that fold upon binding of cAMP and TRIP8b$_{nano}$ are shown in red. (Bottom) Chemical Shift Index (CSI, calculated using TALOS+) plotted as a function of the residue number of CNBD bound to TRIP8b$_{nano}$. Positive values represent helical propensity, while negative values represent strands.

B Ribbon representation of the 10 lowest energy conformers of CNBD bound to TRIP8b$_{nano}$ used for *in silico* modelling of CNBD-TRIP8b$_{nano}$ complex. Secondary structure elements

bioRxiv preprint doi: https://doi.org/10.1101/253096; this version posted January 24, 2018. The copyright holder for this preprint (which was not certified by peer review) is the author/funder, who has granted bioRxiv a license to display the preprint in perpetuity. It is made available under aCC-BY-NC-ND 4.0 International license.

are coloured in light gray and labelled. Loop regions are coloured in dark gray. The distal region of the C-helix (residues 657-662), which is unfolded in the free form of the CNBD (Saponaro *et al*, 2014) and folds upon TRIP8b$_{nano}$ binding, is coloured in red. The unfolded regions at the N- and C-termini of the construct (residues 521–532 and 663 – 672 respectively) are omitted for clarity.

bioRxiv preprint doi: https://doi.org/10.1101/253096; this version posted January 24, 2018. The copyright holder for this preprint (which was not certified by peer review) is the author/funder, who has granted bioRxiv a license to display the preprint in perpetuity. It is made available under aCC-BY-NC-ND 4.0 International license.

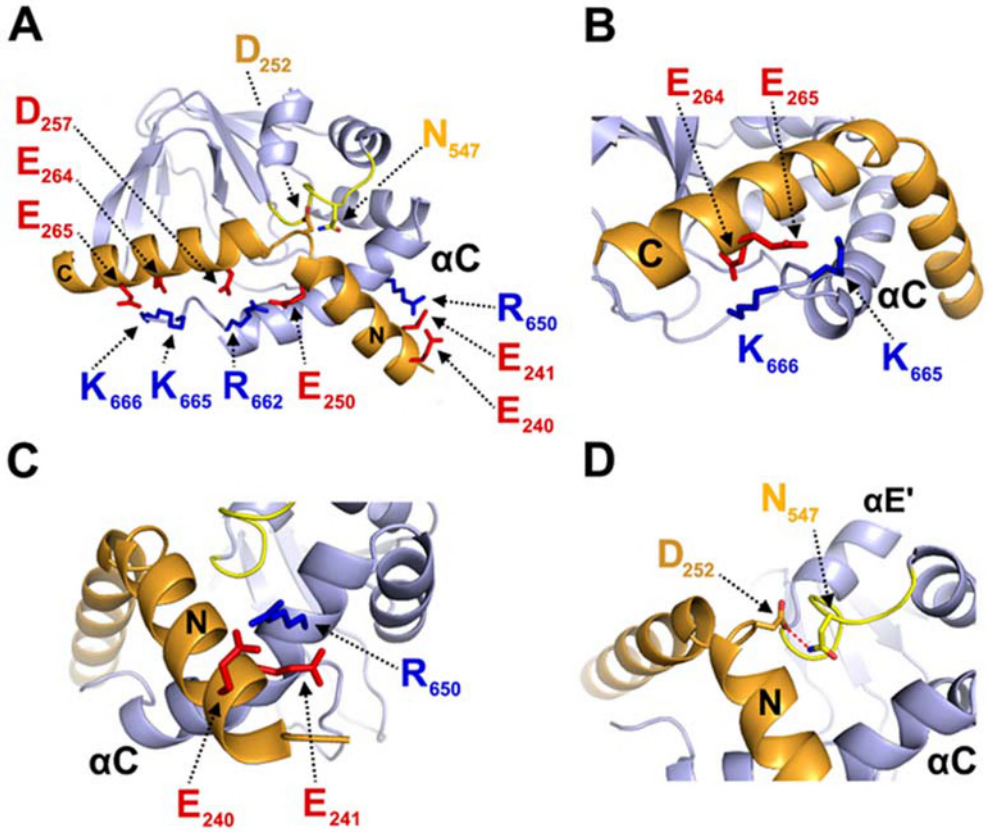

Figure 3. Structural model of CNBD–TRIP8b$_{nano}$ complex.

A Ribbon representation of the complex where CNBD is in gray and TRIP8b$_{nano}$ is in orange. Helix N (N) and helix C (C) of TRIP8b$_{nano}$ are labelled. C-helix of CNBD (αC) is labelled, while N-bundle loop is coloured in yellow. Positively charged residues of C-helix CNBD (blue) and negatively charged residues of TRIP8b$_{nano}$ (red) involved in salt bridges are shown as sticks and labelled. N$_{547}$ of the N-bundle loop (yellow) and D$_{252}$ of TRIP8b$_{nano}$ (orange) are shown as sticks and labelled.

B Close view of K$_{665}$ and K$_{666}$ of CNBD that interact respectively with E$_{265}$ and E$_{264}$ of TRIP8b$_{nano}$. C-helix (αC) of CNBD, and Helix C (C) of TRIP8b$_{nano}$ are labelled.

C Close view of R$_{650}$ of CNBD that is positioned between E$_{240}$ and E$_{241}$ of TRIP8b$_{nano}$. C-helix (αC) of CNBD, and Helix N (N) of TRIP8b$_{nano}$ are labelled.

D Close view of N$_{547}$ of N-bundle loop that forms a hydrogen bond (red dashed line) with D$_{252}$ of TRIP8b$_{nano}$. Helix E' (αE') and C-helix (αC) of CNBD, and Helix N (N) of TRIP8b$_{nano}$ are labelled.

bioRxiv preprint doi: https://doi.org/10.1101/253096; this version posted January 24, 2018. The copyright holder for this preprint (which was not certified by peer review) is the author/funder, who has granted bioRxiv a license to display the preprint in perpetuity. It is made available under aCC-BY-NC-ND 4.0 International license.

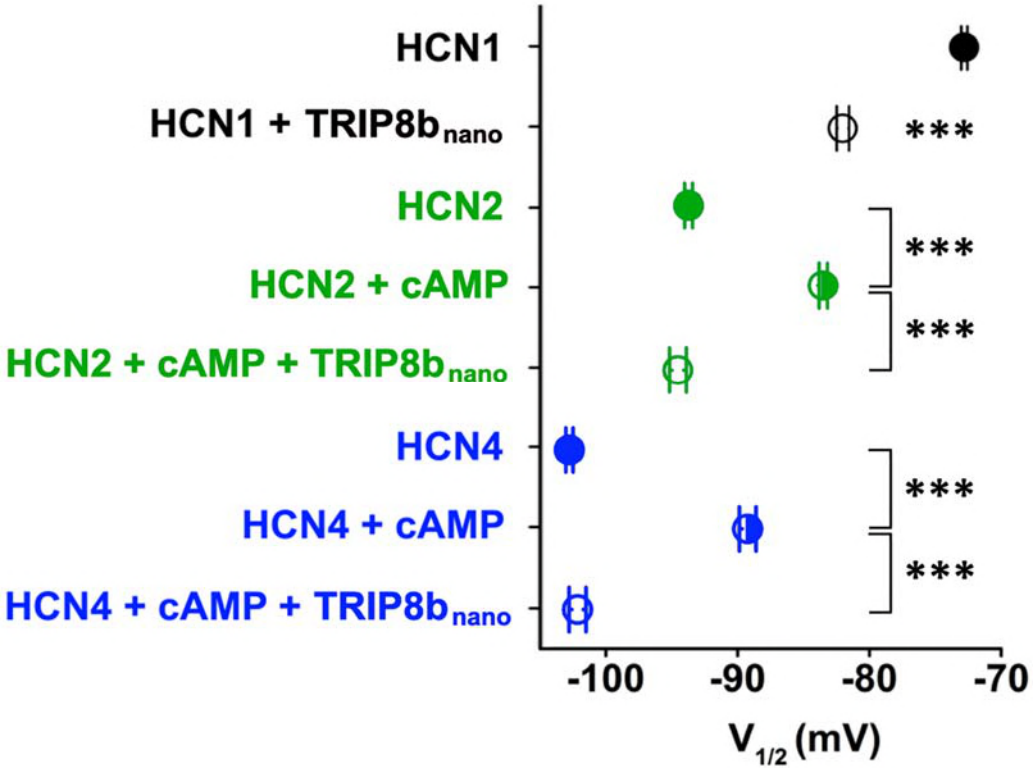

Figure 4. TRIP8b$_{nano}$ abolishes cAMP effect on HCN channel gating.

Effect of TRIP8b$_{nano}$ on human HCN1, mouse HCN2 and rabbit HCN4 half activation potentials ($V_{1/2}$). Half activation potential ($V_{1/2}$) was determined as described in Material and Methods. HCN1 (black filled circle) = -72.8 ± 0.2 mV; HCN1 + 10 µM TRIP8b$_{nano}$ (black open circle) = -82 ± 0.5 mV; HCN2 (green filled circle) = -93.7± 0.3 mV; HCN2 + 5 µM cAMP (green semi-open circle) = -83.5 ± 0.3 mV; HCN2 + 5 µM cAMP + 10 µM TRIP8b$_{nano}$ (green open circle) = -94.5 ± 0.6 mV; HCN4 (blue filled circle) = -102.8 ± 0.3 mV; HCN4 + 1µM cAMP (blue semi-open circle) = -89.2 ± 0.6 mV; HCN4 + 1µM cAMP + 10 µM TRIP8b$_{nano}$ (blue open circle) = -102.1 ± 0.6 mV. Data are presented as mean ± SEM. Number of cells (N) ≥ 11. Statistical analysis performed with ANOVA, followed by post-hoc Tukey test (***, $P < 0.001$).

bioRxiv preprint doi: https://doi.org/10.1101/253096; this version posted January 24, 2018. The copyright holder for this preprint (which was not certified by peer review) is the author/funder, who has granted bioRxiv a license to display the preprint in perpetuity. It is made available under aCC-BY-NC-ND 4.0 International license.

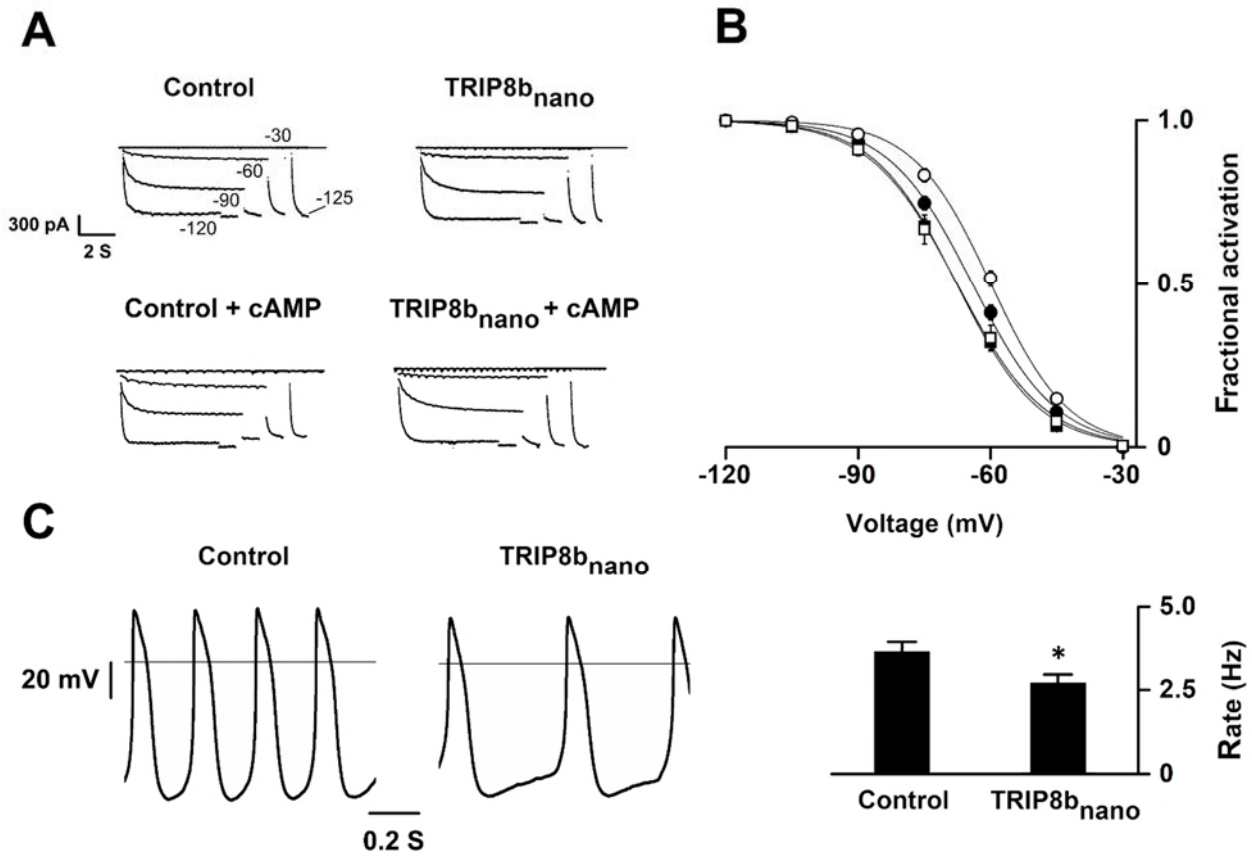

Figure 5. Effects of TRIP8b$_{nano}$ on voltage-dependent activation of I_f and spontaneous rate in rabbit sinoatrial node (SAN) myocytes.

A Representative whole-cell I_f currents recorded, at the indicated voltages, in the control solution and in the presence of 10 μM TRIP8b$_{nano}$, without (top) and with 1 μM cAMP in the pipette (bottom).

B Mean I_f activation curves measured in control (filled circles) or in the presence of: 1 μM cAMP (open circles); 10 μM TRIP8b$_{nano}$ (filled squares); 1 μM cAMP + 10 μM TRIP8b$_{nano}$ (open squares). Ligands were added in the patch pipette. Half activation potential ($V_{1/2}$) of I_f activation curves measured in control = -64.1 ± 0.4 mV or in the presence of: 1 μM cAMP = -59.9 ± 0.4 mV; 10 μM TRIP8b$_{nano}$ = -67.7 ± 0.4 mV; 1 μM cAMP + 10 μM TRIP8b$_{nano}$ = -67.6 ± 0.7 mV. Data are presented as mean ± SEM. Number of cells (N) was ≥ 15. $V_{1/2}$ values are significantly different between each other's whit the exception of $V_{1/2}$ obtained in the presence TRIP8b$_{nano}$ and cAMP + TRIP8b$_{nano}$. Statistical analysis performed with ANOVA, followed by post-hoc Bonferroni test (*, $P < 0.05$)

C (Left) Representative recordings of single SAN cell spontaneous activity in control and in the presence of 10 μM TRIP8b$_{nano}$. (Right) Mean spontaneous rate (Hz) recorded in

bioRxiv preprint doi: https://doi.org/10.1101/253096; this version posted January 24, 2018. The copyright holder for this preprint (which was not certified by peer review) is the author/funder, who has granted bioRxiv a license to display the preprint in perpetuity. It is made available under aCC-BY-NC-ND 4.0 International license.

control solution = 3.65 ± 0.29 Hz and in the presence of 10 μM TRIP8b$_{nano}$ added to the pipette = 2.69 ± 0.27 Hz. Data are presented as mean ± SEM. Number of cells (N) was ≥ 7. Statistical analysis performed with t test (*, $P < 0.05$).

bioRxiv preprint doi: https://doi.org/10.1101/253096; this version posted January 24, 2018. The copyright holder for this preprint (which was not certified by peer review) is the author/funder, who has granted bioRxiv a license to display the preprint in perpetuity. It is made available under aCC-BY-NC-ND 4.0 International license.

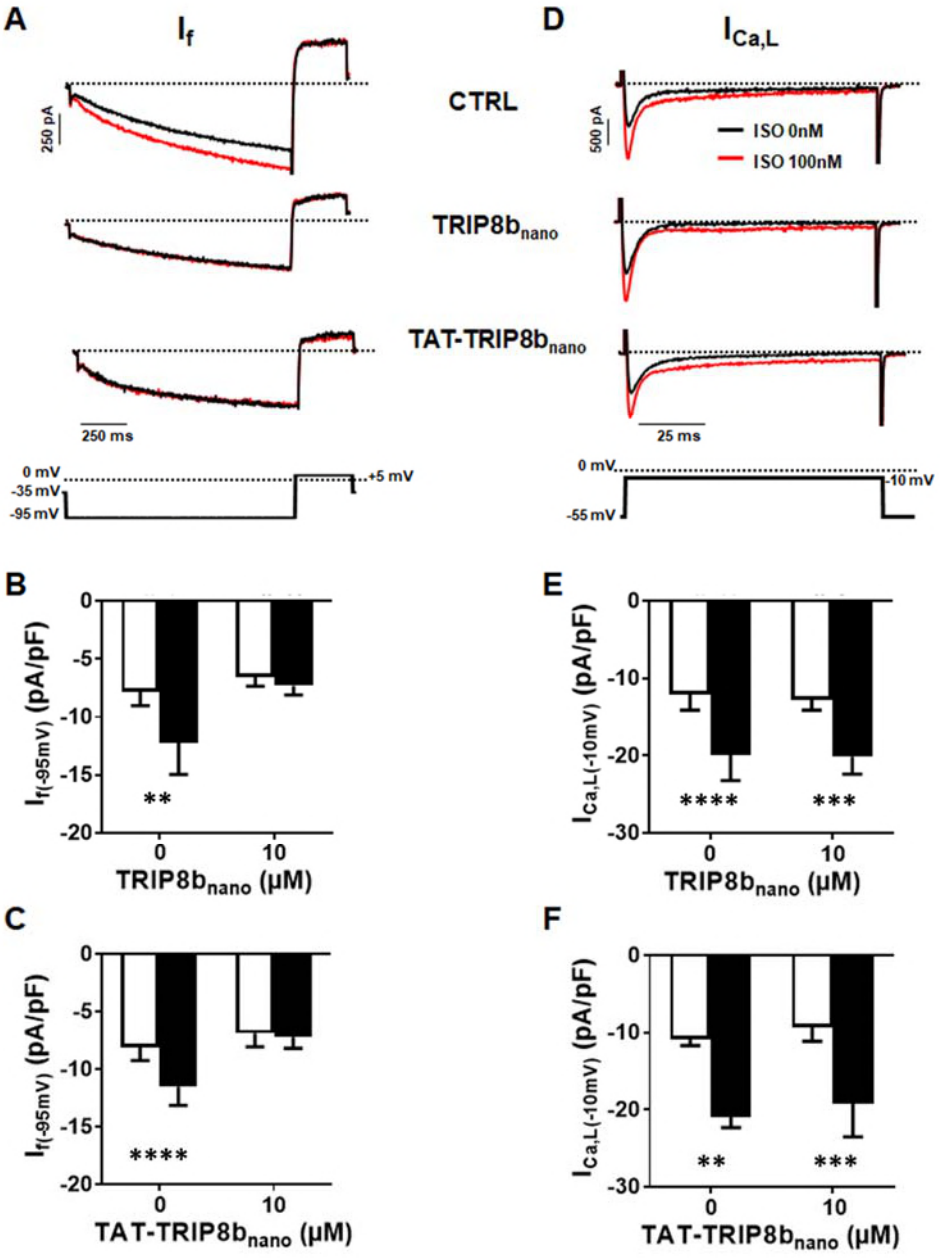

Figure 6. Effect of TRIP8b$_{nano}$ and TAT-TRIP8b$_{nano}$ on I_f and $I_{Ca,L}$ in mouse sinoatrial node (SAN) myocytes.

A Representative examples of I_f recordings at -95 mV in control conditions (top), in 10 µM TRIP8b$_{nano}$ dialysed cell (middle) and in cells perfused with 10 µM TAT-TRIP8b$_{nano}$ (bottom), before (black trace) and after (red trace) application of ISO 100 nM. The voltage-clamp protocol used for recordings is shown above current traces.

B Mean normalised I_f current density recorded at -95 mV in absence and in presence of 10 µM TRIP8b$_{nano}$ in the patch pipette, before (open bars) and after (filled bars) 100 nM ISO perfusion. Data are presented as mean ± SEM. Number of cells (N) ≥ 6. Statistical

bioRxiv preprint doi: https://doi.org/10.1101/253096; this version posted January 24, 2018. The copyright holder for this preprint (which was not certified by peer review) is the author/funder, who has granted bioRxiv a license to display the preprint in perpetuity. It is made available under aCC-BY-NC-ND 4.0 International license.

analysis performed with two-way ANOVA test, followed by Sidak multiple comparisons test (**, P < 0.01).

C Mean normalised I_f current density recorded at -95 mV in control solution or in the solution containing 10 µM TAT-TRIP8b$_{nano}$, in absence (open bars) and in the presence (filled bars) of 100 nM ISO. Data are presented as mean ± SEM. Number of cells (N) ≥ 8. Statistical analysis performed with two-way ANOVA test, followed by Sidak multiple comparisons test (****, P < 0.0001).

D Representative examples of $I_{Ca,L}$ recordings at -10 mV in control conditions (top), in 10µM TRIP8b$_{nano}$ dialysed cell (middle) and in cells perfused with 10 µM TAT-TRIP8b$_{nano}$ (bottom), before (black trace) and after (red trace) application of ISO 100 nM. The voltage-clamp protocol used for recordings is shown above current traces.

E Mean normalised $I_{Ca,L}$ current density recorded at -10 mV in absence and in presence of 10 µM TRIP8b$_{nano}$ in the patch pipette, before (open bars) and after (filled bars) 100 nM ISO perfusion. Data are presented as mean ± SEM. Number of cells (N) ≥ 8. Statistical analysis performed with two-way ANOVA test, followed by Sidak multiple comparisons test (***, P < 0.001; ****, P < 0.0001).

F Mean normalised $I_{Ca,L}$ current density recorded at -10 mV in control solution or in the solution containing 10 µM TAT-TRIP8b$_{nano}$, in absence (open bars) and in the presence (filled bars) of 100 nM ISO. Data are presented as mean ± SEM. Number of cells (N) ≥ 7. Statistical analysis performed with two-way ANOVA test, followed by Sidak multiple comparisons test (**, P < 0.01; *** P < 0.001).

bioRxiv preprint doi: https://doi.org/10.1101/253096; this version posted January 24, 2018. The copyright holder for this preprint (which was not certified by peer review) is the author/funder, who has granted bioRxiv a license to display the preprint in perpetuity. It is made available under aCC-BY-NC-ND 4.0 International license.

Supporting Information

- Appendix Fig S1. **CNBD residues involved in TRIP8b$_{nano}$ binding.**
- Appendix Fig S2. **Representative families of clusters obtained from the first docking calculation.**
- Appendix Fig S3. **Biochemical validation of CNBD – TRIP8b$_{nano}$ complex.**
- Appendix Fig S4. **Different orientation of R$_{662}$ and K$_{665}$ in the cAMP-bound and TRIP8b$_{nano}$-bound conformation of the CNBD.**
- Appendix Fig S5. **Comparison of half activation potentials of human HCN1 WT and of the cAMP-insensitive R$_{549}$E mutant in the absence and in the presence of cAMP.**
- Appendix Table S1. **Acquisition parameters for NMR experiments performed on cAMP-free human HCN2 CNBD in complex with TRIP8b$_{nano}$ and vice-versa.**
- Appendix Table S2. **Docking calculation.**

bioRxiv preprint doi: https://doi.org/10.1101/253096; this version posted January 24, 2018. The copyright holder for this preprint (which was not certified by peer review) is the author/funder, who has granted bioRxiv a license to display the preprint in perpetuity. It is made available under aCC-BY-NC-ND 4.0 International license.

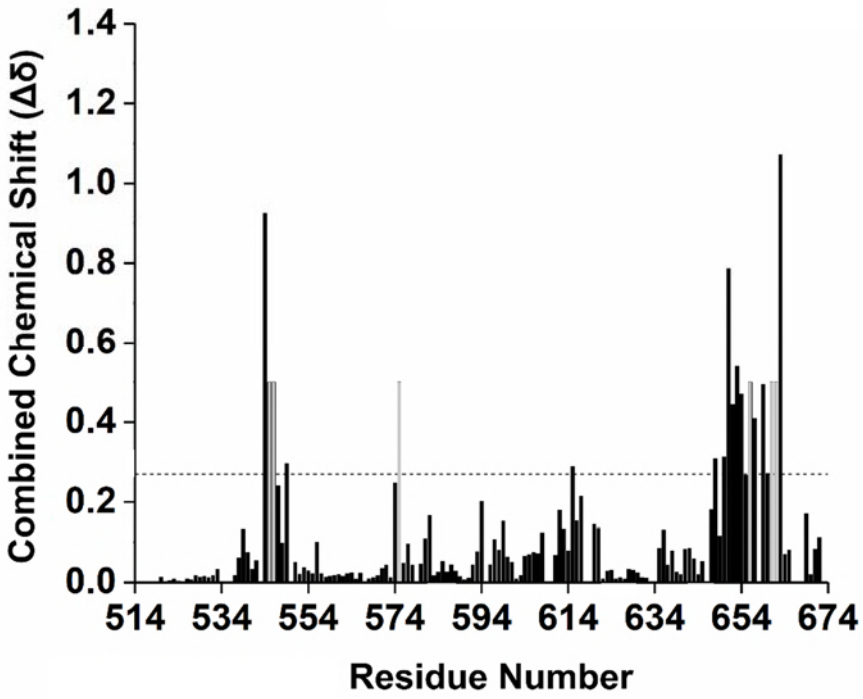

Appendix Fig S1. CNBD residues involved in TRIP8b$_{nano}$ binding.

Combined chemical shift variations of NMR signals between CNBD unbound and TRIP8b$_{nano}$-bound state. Combined chemical shift variations are calculated from the experimental ^{1}H and ^{15}N chemical shift changes (Δδ(^{1}H) and Δδ (^{15}N), respectively) between the corresponding peaks in the two forms, through the following equation (Garrett *et al*, 1997).

$$\Delta\delta^{combined} = \sqrt{\frac{\left(\Delta\delta\left(^{1}\mathrm{H}\right)\right)^{2} + \frac{1}{25}\left(\Delta\delta\left(^{15}\mathrm{N}\right)\right)^{2}}{2}}$$

Residues experiencing intermediate exchange regime (whose NMR signal becomes broad beyond detection upon addition of TRIP8b$_{nano}$) are shown in grey. The horizontal dotted line indicates the average value plus one standard deviation. Residues above the line were set as “active” in the docking calculation described in the text (see Materials and Methods).

Garrett DS, Seok YJ, Peterkofsky A, Clore GM & Gronenborn AM (1997) Identification by NMR of the binding surface for the histidine-containing phosphocarrier protein HPr on the N-terminal domain of enzyme I of the Escherichia coli phosphotransferase system. *Biochemistry* **36:** 4393–4398

bioRxiv preprint doi: https://doi.org/10.1101/253096; this version posted January 24, 2018. The copyright holder for this preprint (which was not certified by peer review) is the author/funder, who has granted bioRxiv a license to display the preprint in perpetuity. It is made available under aCC-BY-NC-ND 4.0 International license.

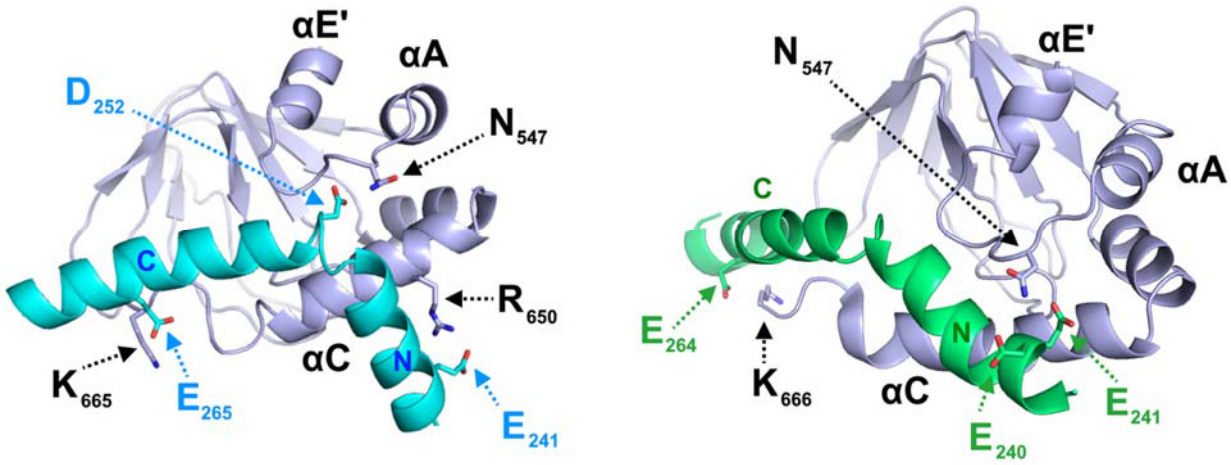

Appendix Fig S2. Representative families of clusters obtained from the first docking calculation.

The clusters obtained can be grouped in two classes, shown here, on the basis of the position of helix N of TRIP8b$_{nano}$ (N) relative to the CNBD. In the left representative structure, helix N is oriented in a way that allows E_{241} to interact with R_{650} of C-helix. In the right representative structure, E_{240} - E_{241} interact with N_{547} of CNBD. In all clusters K_{665} or K_{666} of CNBD establish a contact with either E_{264} or E_{265} of TRIP8b$_{nano}$. The structural elements of CNBD are labelled: αE', αA and αC. Helices N and C of TRIP8b$_{nano}$ are labelled.

bioRxiv preprint doi: https://doi.org/10.1101/253096; this version posted January 24, 2018. The copyright holder for this preprint (which was not certified by peer review) is the author/funder, who has granted bioRxiv a license to display the preprint in perpetuity. It is made available under aCC-BY-NC-ND 4.0 International license.

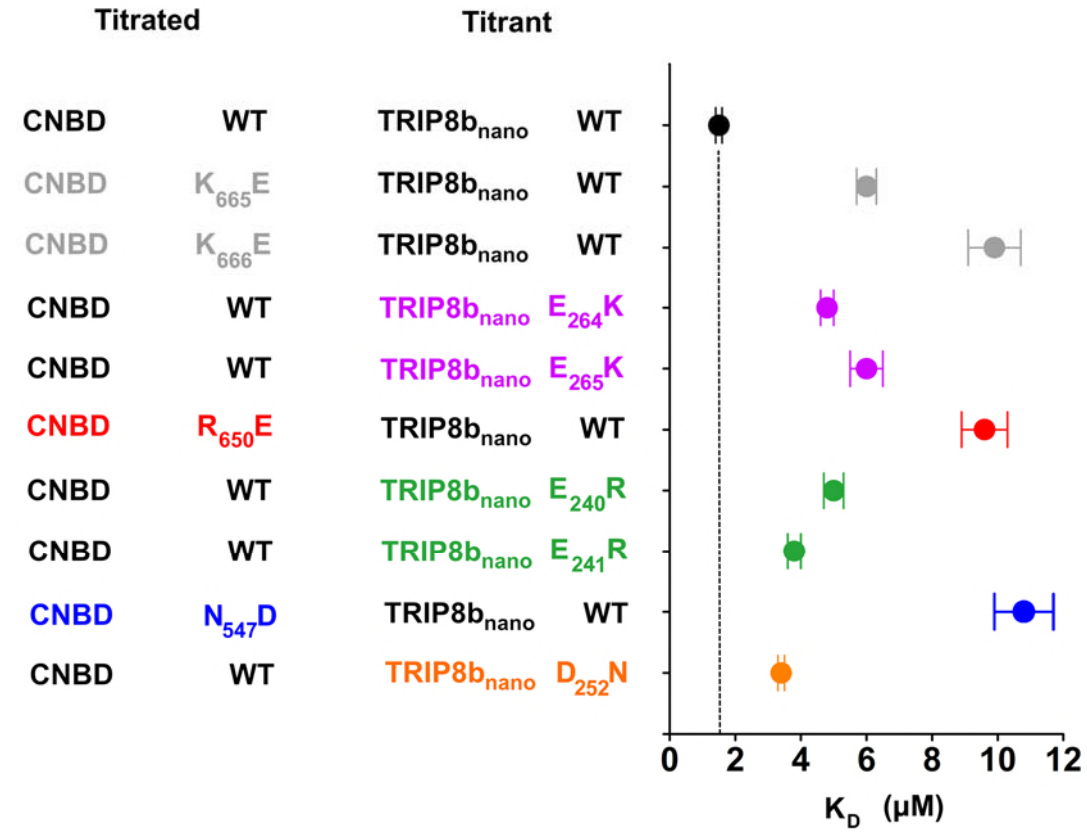

Appendix Fig S3. Biochemical validation of CNBD – TRIP8b$_{nano}$ complex.

Dissociation constant (K_D) of the interaction between the indicated CNBD and TRIP8b$_{nano}$ peptides were measured by means of Isothermal Titration Calorimetry (ITC). CNBD WT - TRIP8b$_{nano}$ WT (black filled circle) = 1.4 ± 0.1 μM; CNBD K$_{665}$E - TRIP8b$_{nano}$ WT (grey filled circle) = 6 ± 0.3 μM; CNBD K$_{666}$E - TRIP8b$_{nano}$ WT (grey filled circle) = 9.9 ± 0.8 μM; CNBD WT - TRIP8b$_{nano}$ E$_{64}$K (purple filled circle) = 4.8 ± 0.2 μM; CNBD WT - TRIP8b$_{nano}$ E$_{65}$K (purple filled circle) = 6 ± 0.5 μM; CNBD R$_{650}$E - TRIP8b$_{nano}$ WT (red filled circle) = 9.6 ± 0.7 μM; CNBD WT - TRIP8b$_{nano}$ E$_{40}$R (green filled circle) = 5 ± 0.3 μM; CNBD WT - TRIP8b$_{nano}$ E$_{41}$R (green filled circle) = 3.8 ± 0.2 μM; CNBD N$_{547}$D - TRIP8b$_{nano}$ WT (blue filled circle) = 11 ± 0.9 μM; CNBD WT - TRIP8b$_{nano}$ D$_{52}$N (orange filled circle) = 3.4 ± 0.1 μM. Data are presented as mean ± SEM. Number of experiments (N) ≥ 3. K_D values of all tested combinations are statistically different from the K_D of CNBD WT for TRIP8b$_{nano}$ WT (*, $P \leq 0.05$; **, $P < 0.01$). Statistical analysis performed with ANOVA, followed by post-hoc Tukey test. Dashed black vertical line indicates the K_D of WT peptides.

bioRxiv preprint doi: https://doi.org/10.1101/253096; this version posted January 24, 2018. The copyright holder for this preprint (which was not certified by peer review) is the author/funder, who has granted bioRxiv a license to display the preprint in perpetuity. It is made available under aCC-BY-NC-ND 4.0 International license.

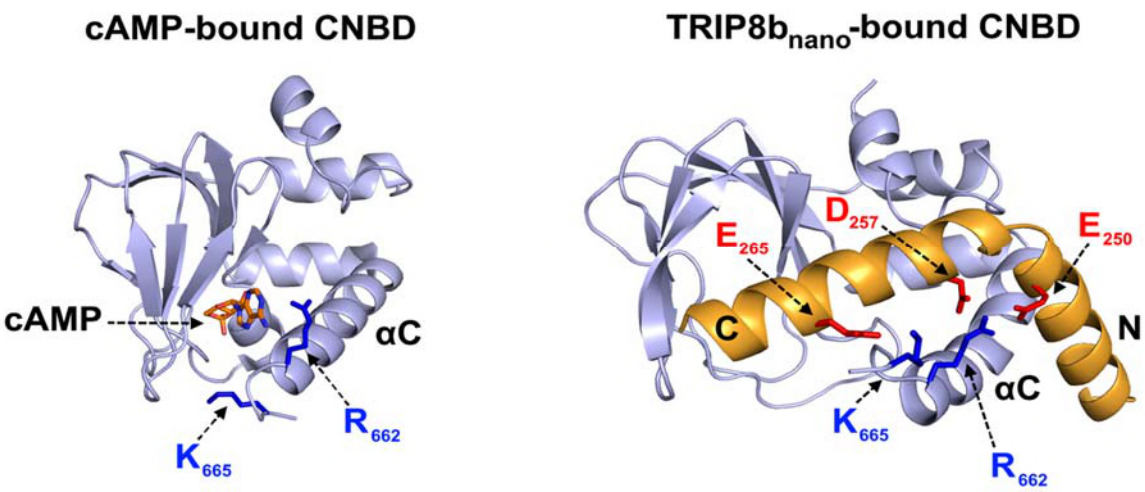

Appendix Fig S4. Different orientation of R_{662} and K_{665} in the cAMP-bound and TRIP8b$_{nano}$-bound conformation of the CNBD.

Residues R_{662} and K_{665} of CNBD C-helix (αC) which interact with cAMP (left, (Lolicato *et al*, 2011) and TRIP8b$_{nano}$ (right, this study) are represented as blue sticks and labelled. TRIP8b$_{nano}$ residues E_{250} and D_{257} interacting with R_{662} and residue E_{265} interacting with K_{665} are shown in red sticks and labelled.

Lolicato M, Nardini M, Gazzarrini S, Moller S, Bertinetti D, Herberg FW, Bolognesi M, Martin H, Fasolini M, Bertrand JA, Arrigoni C, Thiel G & Moroni A (2011) Tetramerization dynamics of C-terminal domain underlies isoform-specific cAMP gating in hyperpolarization-activated cyclic nucleotide-gated channels. *J. Biol. Chem.* **286:** 44811–44820

bioRxiv preprint doi: https://doi.org/10.1101/253096; this version posted January 24, 2018. The copyright holder for this preprint (which was not certified by peer review) is the author/funder, who has granted bioRxiv a license to display the preprint in perpetuity. It is made available under aCC-BY-NC-ND 4.0 International license.

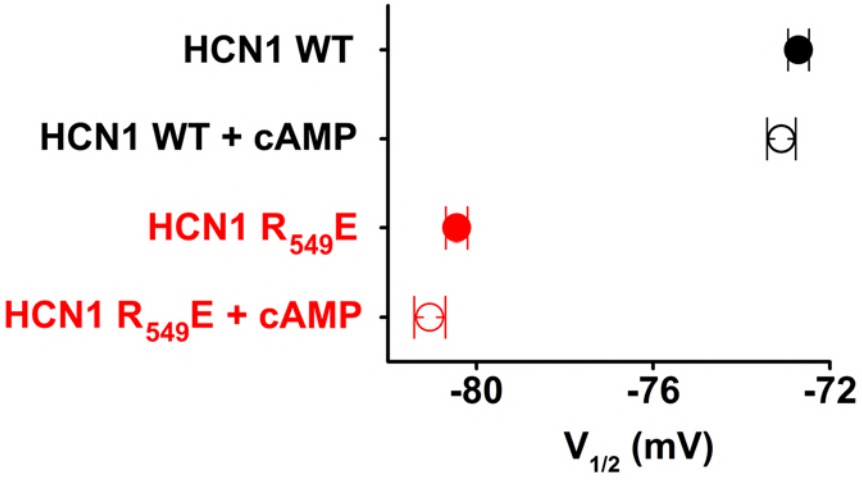

Appendix Fig S5. Comparison of half activation potentials of human HCN1 WT and of the cAMP-insensitive $R_{549}E$ mutant in the absence and in the presence of cAMP.

Currents were measured by patch clamp from HEK 293T cells transfected with WT and $R_{549}E$ mutant (Chen *et al*, 2001) in the absence and presence of 15 µM cAMP in the pipette. Half activation potential ($V_{1/2}$) was determined as described in Material and Methods. HCN1 WT (black filled circle) = -72.7 ± 0.2 mV; HCN1 WT + cAMP (black open circle) = 73.1 ± 0.3 mV; HCN1 $R_{549}E$ (red filled circle) = -80.4 ± 0.2 mV; HCN1 $R_{549}E$ + cAMP (red open circle) = -81 ± 0.3 mV. Data are presented as mean ± SEM. Number of experiments (N) ≥ 8.

Chen S, Wang J & Siegelbaum SA (2001) Properties of Hyperpolarization-Activated Pacemaker Current Defined by Coassembly of Hcn1 and Hcn2 Subunits and Basal Modulation by Cyclic Nucleotide. *J. Gen. Physiol.* **117:** 491–504 Available at: http://www.jgp.org/lookup/doi/10.1085/jgp.117.5.491

bioRxiv preprint doi: https://doi.org/10.1101/253096; this version posted January 24, 2018. The copyright holder for this preprint (which was not certified by peer review) is the author/funder, who has granted bioRxiv a license to display the preprint in perpetuity. It is made available under aCC-BY-NC-ND 4.0 International license.

Appendix Table S1. Acquisition parameters for NMR experiments performed on cAMP-free human HCN2 CNBD in complex with TRIP8b$_{nano}$ and vice-versa.

Experiments	Dimension of acquired data			Spectral width (ppm)			n[a]
	t_1	t_2	t_3	F_1	F_2	F_3	
HCN2 CNBD [b]							
^{1}H-^{15}N-HSQC	256(^{15}N)	1024(^{1}H)		32	16		8
CBCA(CO)NH	108(^{13}C)	56(^{15}N)	2048(^{1}H)	72	32	16	16
HNCACB	108(^{13}C)	56(^{15}N)	2048(^{1}H)	72	32	16	16
HNCO	80(^{13}C)	56(^{15}N)	2048(^{1}H)	18	32	16	4
HN(CA)CO	80(^{13}C)	56(^{15}N)	2048(^{1}H)	18	32	16	16
^{15}N-edited [^{1}H-^{1}H]-NOESY[c]	192(^{1}H)	74(^{15}N)	2048(^{1}H)	14	70	14	16
TRIP8bnano[d]							
^{1}H-^{15}N-HSQC	128(^{15}N)	1024(^{1}H)		40	14		16
CBCA(CO)NH	88(^{13}C)	48(^{15}N)	2048(^{1}H)	80	40	16	24
HNCACB	88(^{13}C)	48(^{15}N)	2048(^{1}H)	80	40	16	24
HNCA	88(^{13}C)	48(^{15}N)	1024(^{1}H)	50	40	16	24
HN(CO)CA	88(^{13}C)	48(^{15}N)	1024(^{1}H)	50	40	16	24

[a] number of acquired scans. [b] Experiments were acquired on a 700 MHz Bruker spectrometer equipped with a triple resonance cryoprobe at 298 K. All the triple resonance (TCI 5-mm) probes used were equipped with Pulsed Field Gradients along the z-axis.
[c] ^{15}N-edited edited 3D NOESY-HSQC experiments was acquired with a mixing time value of 100ms at the Bruker Avance 950 MHz spectrometer. [d] Experiments were acquired on a 500 MHz Bruker spectrometer equipped with a triple resonance cryoprobe at 298 K. All 3D and

bioRxiv preprint doi: https://doi.org/10.1101/253096; this version posted January 24, 2018. The copyright holder for this preprint (which was not certified by peer review) is the author/funder, who has granted bioRxiv a license to display the preprint in perpetuity. It is made available under aCC-BY-NC-ND 4.0 International license.

2D spectra were processed using the standard Bruker software TOPSPIN 2.1 and analyzed through CARA (Keller R *et al*, 2002; Keller RLJ. 2004).

Keller R, Wüthrich KA. (2002) New Software for the Analysis of Protein NMR Spectra.
Keller RLJ. (2004) The Computer Aided Resonance Assignment tutorial. Goldau: CANTINA Verlag.

Appendix Table S2. Docking calculation.

HADDOCK Score [b]	-130 (7)
RMSD (Å) [c]	1.8 (0.9)
Number of structures	71
BSA (Å^2) [d]	1968 (106)
EAIR [e]	30.5 (15.2)
Einter[f]	-398(50)
Enb[g]	-431(46)

Statistics on the top-ranking cluster of the structural models of CNBD and TRIP8b$_{nano}$ complex obtained through HADDOCK2.2 calculations and in agreement with previous experimental data (Deberg *et al*, 2015). Averages (standard deviations are reported in parenthesis) were calculated over the best ten structures.

[a] Cluster rank according to the HADDOCK score. [b] HADDOCK score defined as a weighted sum of different energetic terms, such as: van der Waals energy, electrostatic energy, distance restraints energy, buried surface area, binding energy and desolvation energy. [c] Backbone RMSD from the lowest HADDOCK score structure in each cluster. Some individual energy terms are also reported: [d] Buried surface area, [e] distance restraints energy, [f] binding energy, [g] non-bonded interaction energy.

Deberg HA, Bankston JR, Rosenbaum JC, Brzovic PS, Zagotta WN & Stoll S (2015) Structural mechanism for the regulation of HCN ion channels by the accessory protein TRIP8b. *Structure* **23:** 734–744